

Seismic monitoring and analysis of deep geothermal projects in St Gallen and Basel, Switzerland

Benjamin Edwards,* Toni Kraft, Carlo Cauzzi, Philipp Kästli and Stefan Wiemer

Swiss Seismological Service, ETH, Zürich, Switzerland. E-mail: edwards@sed.ethz.ch

Accepted 2015 February 5. Received 2015 February 4; in original form 2014 September 16

SUMMARY

Monitoring and understanding induced seismicity is critical in order to estimate and mitigate seismic risk related to numerous existing and emerging techniques for natural resource exploitation in the shallow-crust. State of the art approaches for guiding decision making, such as traffic light systems, rely heavily on data such as earthquake location and magnitude that are provided to them. In this context we document the monitoring of a deep geothermal energy project in St Gallen, Switzerland. We focus on the issues of earthquake magnitude, ground motion and macroseismic intensity which are important components of the seismic hazard associated to the project. We highlight the problems with attenuation corrections for magnitude estimation and site amplification that were observed when trying to apply practices used for monitoring regional seismicity to a small-scale monitoring network. Relying on the almost constant source-station distance for events in the geothermal ‘seismic cloud’ we developed a simple procedure, calibrated using several $M_L > 1.3$ events, which allowed the unbiased calculation of M_L using only stations of the local monitoring network. The approach determines station specific M_L correction terms that account for both the bias of the attenuation correction in the near field and amplification at the site. Since the smallest events ($M_L < -1$) were only observed on a single borehole instrument, a simple relation between the amplitude at the central borehole station of the monitoring network and M_L was found. When compared against magnitudes computed over the whole network this single station approach was shown to provide robust estimates (± 0.17 units) for the events down to $M_L = -1$. The relation could then be used to estimate the magnitude of even smaller events ($M_L < -1$) only recorded on the central borehole station. Using data from almost 2700 events in Switzerland, we then recalibrated the attenuation correction, extending its range of validity from a minimum source–station distance of 20 km down to 1 km. Based on this we could determine the component of the previously derived station specific M_L corrections due to local amplification. We analysed ground-motion and detailed macroseismic reports resulting from the 2013 July 20 St Gallen $M_L = 3.5 \pm 0.1$ ($M_w = 3.3\text{--}3.5 \pm 0.1$) ‘main shock’ and compared it to a similar $M_L = 3.4 \pm 0.1$ event ($M_w = 3.2 \pm 0.1$) that occurred in 2006 at another deep geothermal project in Basel, Switzerland. Differences in ground motion amplitudes between the Basel and St Gallen events and to an extent, the associated macroseismic observations, were investigated in terms of the different source terms: M_w for long-period motions and the source-corner frequency (related to the source rupture velocity and stress-drop) for short periods.

Key words: Earthquake ground motions; Earthquake source observations; Seismic attenuation; Site effects.

INTRODUCTION

Induced seismicity is a topic of growing debate, whether related to geothermal energy, shale-gas extraction or CO₂ storage. The

need to satisfy increasing energy demands whilst considering environmental impact and legislation means that efficient sources of energy and storage of CO₂ are in great demand. Traditional renewable sources (hydroelectric, solar, wind etc.) provide for a degree of the increasing energy demand, but one of the most promising fields is the exploitation of the Earth’s upper crust for geothermal energy (Fridleifsson 2001). Exploitation of these natural resources in the upper-crust, in particular geothermal energy, is however, not

*Now at: Department of Earth, Ocean and Ecological Sciences, University of Liverpool, Liverpool L69 3GP, United Kingdom.

without drawbacks. A main topic of debate is related to the triggering of seismicity. Induced earthquakes related to geothermal energy are mainly related to changes in pore pressure (Kisslinger 1976; Ellsworth 2013). Hydrothermal (as opposed to ‘enhanced’) geothermal systems are deployed in areas suspected to accommodate a suitable subsurface reservoir and often target fault zones that promise naturally enhanced permeability. Therefore, in addition to seismicity directly related to pore-pressure changes inside the geothermal reservoir, the subsequent interaction of fluids with pre-existing faults may lead to fault weakening (e.g. Blanpied *et al.* 1992; Faulkner *et al.* 2010), and, in the case of sufficient tectonic pre-loading, potentially trigger more significant seismicity.

Clearly, seismic monitoring of projects that may trigger shallow seismicity is important and will facilitate and further the understanding of geomechanical processes in the upper-crust. Furthermore, effective monitoring is particularly necessary for geothermal projects, with plants typically sited near to populated areas: the production of heated water in addition to electricity increasing economic viability. Whilst the largest earthquakes associated with geothermal systems are typically only moderate in size, the proximity to infrastructure and local population introduces significant risk. For instance, an enhanced geothermal system (EGS) in Basel led to insured damage claims of \$7.5 M and total costs of \$9 M after a $M_w = 3.2$ event occurred at a depth of less than 5 km within the city (Geo Explorers Ltd., personal communication, 2012; Giardini 2009).

The robust and consistent computation of earthquake location and magnitude is an important aspect of seismic monitoring and analysis. The reliable dissemination of this information is crucial to many branches of seismology since earthquake catalogues are used for numerous subsequent scientific studies. In the case of projects where hazard is monitored in real-time (e.g. geothermal or mining operations), such information should be ideally integrated into automated monitoring and analysis systems [e.g. traffic light systems (TLSs)]. For example, the determination of event recurrence (parametrization of the Gutenberg & Richter 1944 relation) is critical for predicting the probability of future earthquakes exceeding a threshold magnitude (e.g. Henderson *et al.* 1999; Shapiro *et al.* 2007; Bachmann *et al.* 2011).

The principal of the TLS (Bommer *et al.* 2006) has been adopted in many studies due to its simplicity and effectiveness for operational decision making. The system provides a clear approach for policy decisions to be made, such as defining acceptable levels of shaking or disturbance, and assigning actions to their exceedance. In order to successfully follow such systems it is important that the monitoring effort is appropriate. For the original, purely reactive TLS, operational decisions were linked to instrumental observations such as peak ground-motions (PGV). Such approaches require a rather simple monitoring system. For example, an approach based on the TLS was implemented in the Basel enhanced geothermal project (Håring *et al.* 2008), with alerts based on a combination of (i) public response; (ii) local magnitude (M_L) and (iii) PGV. In the case of Advanced TLS, which aim to include geomechanical modelling and forecasting (e.g. Taron & Ellsworth 2009; Cloetingh *et al.* 2010; Goertz-Allmann & Wiemer 2012; Gischig & Wiemer 2013), the monitoring effort must be able to accurately monitor the development of features such as fluid migration, preferential fault activation, and 3-D distribution of the frequency-magnitude distribution of seismicity. While clearly requiring a more exhaustive monitoring solution, such approaches will allow better understanding and management of the geothermal system, and potential associated hazards.

In this paper we show an example of the monitoring and interpretation of seismicity by the Swiss Seismological Service (SED) associated to the St Gallen, Switzerland, deep geothermal project. In the following, we briefly describe the history of the induced earthquake sequence observed during this project. Further information can be found in Diehl *et al.* (2014). The project began the drilling phase in March 2013 and aimed to find and exploit potential hydrothermal aquifers in the Mesozoic layers of the Molasse Basin. A small-scale injection test using fresh water on July 14 was followed by two stages of acid stimulation on July 17. A low-level of micro-seismicity that strongly correlated with the testing and stimulation program was observed by the SED on a dedicated network of 10 surface stations and one shallow borehole station (at a depth of 205 m). When preparing for a production test, gas from an unknown source at depth suddenly entered the well at around noon of July 19. The borehole was closed immediately but the well-head pressure gradually increased to levels that would eventually have endangered well integrity. The operators therefore decided to fight the ‘gas-kick’ by pumping drilling mud into the well to push the gas back into the formation. As soon as injection began, microseismicity restarted in the vicinity of the injection point. Although the TLS designed by the operators was triggered in the early phase of the seismicity increase (July 19, 18:51 UTC), the operators found themselves forced to continue well control instead of stopping the pumps. During this period, the seismicity intensified and culminated in a $M_L = 3.5 \pm 0.1$ event at 3:30 (UTC) on July 20 that was widely felt in the area. Numerous subsequent events have been detected and located by the SED until October 2013, when seismicity was essentially turned off immediately by a long-term production test (Diehl *et al.* 2014).

Due to the small nature of the ‘aftershocks’ of the $M_L = 3.5 \pm 0.1$ event, the presence of amplification effects at several stations, and the apparent breakdown of the attenuation correction relation at distances of less than 20 km, the determination of earthquake magnitudes was not straightforward. This led to an initial overestimation of magnitudes and the related seismic hazard. Both instrumental and macroseismic intensity fields were determined for the main shock and led to interesting comparisons with the Basel EGS ($M_L = 3.4 \pm 0.1$; $M_w = 3.2 \pm 0.1$) event (Baer *et al.* 2007). In the case of the Basel event, with similar magnitude and proximity to the city, widespread minor non-structural damage was reported (Giardini 2009). However, in the case of St Gallen ($M_L = 3.5 \pm 0.1$; Moment Tensor $M_w = 3.3 \pm 0.1$; Spectral $M_w = 3.5 \pm 0.1$; forthwith $M_w = 3.4 \pm 0.1$) almost no damage was reported. Standard hazard and risk assessment approaches use ground motion prediction equations which define for given magnitude and distance an expected shaking level and its uncertainty. The observed disparity of damage in this case is therefore of significant interest.

MONITORING NETWORK

The Swiss national seismic network [comprising the Swiss Digital Seismic Network (SDSNet; Diehl *et al.* 2013) and Strong-Motion Network (Clinton *et al.* 2011)] operated by the SED are relatively sparse in the wider surroundings of St Gallen. Recent estimates of the magnitude of completeness (M_c) find values of M_L 1.6 to M_L 1.7 for the region (Nanjo *et al.* 2010; Kraft *et al.* 2013). With the existing monitoring network the precision of earthquake epicentre location can be estimated to lie in the order of a few kilometres, while the source depth is subject to larger uncertainties. This level of

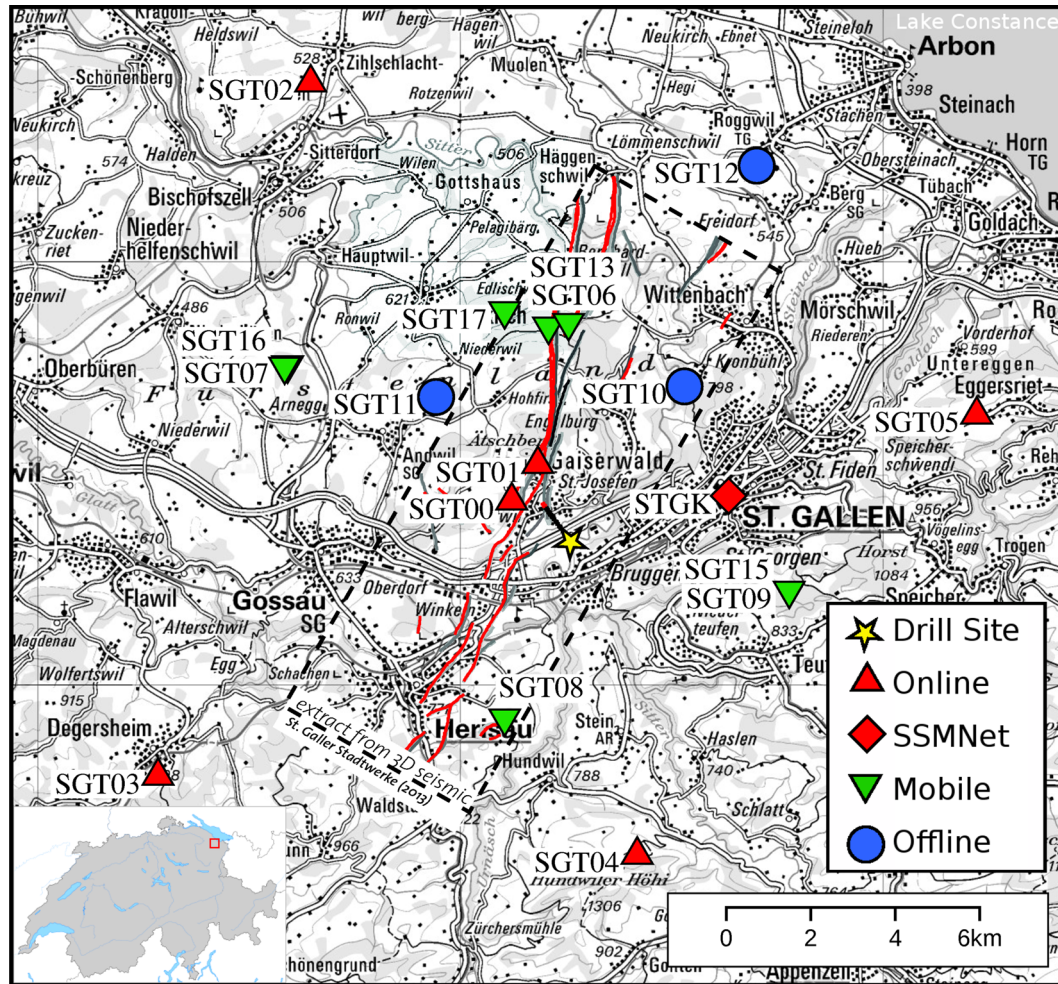


Figure 1. Map of the St. Gallen area, northeast Switzerland. The seismic monitoring network (symbols) and the Sankt Gallen Fault Zone (red lines), as derived by 3-D seismics by Sankt Galler Stadtwerke, are indicated. The surface projection of the wellbore is indicated by a black line extending from the drill site towards the NW. Symbols: red: basic monitoring network; green: mobile stations with real-time data transmission; blue: mobile stations without data transmission.

monitoring was not even sufficient to allow a reliable discrimination of natural and induced seismicity, never mind the subsequent scientific analysis and interpretation of the geothermal system. Consequently, providing near real-time information on induced seismicity to the operator, authorities and public, as well as authoritative input for the TLS run by the operator would not have been possible.

With support of the operator (Sankt Galler Stadtwerke) and of the Swiss Federal Office of Energy, the SED was able to temporally improve the monitoring network in the St. Gallen area significantly. In February 2012 five broad-band stations (SGT0[1–5]) and one shallow borehole station (SGT00, 205 m) were installed at a maximum distance of 12 km from the drill site (Fig. 1). The borehole station and one broad-band station were installed at a distance of 500 m to the surface projection of the planned landing point of the geothermal well. All broad-band stations were installed in the basements of pre-existing structures (2–5 m below the surface) with mains power and real-time communication. To account for the heterogeneous ambient seismic noise field in this densely populated area, the geometry of network was determined by computer-based optimization using the method of Kraft *et al.* (2013). Two accelerometer stations, one in the centre of the city of St. Gallen (STGK) within the Swiss Strong Motion Network (Clinton *et al.* 2011; Cauzzi & Clinton

2013), and one co-located with the borehole station, completed the basic monitoring network (red symbols in Fig. 1).

In early July 2013 four additional short-period stations (SGT[06–09] green symbols in Fig. 1) running on batteries and recording on local flash cards were installed at a distance of about 5 km around the drill site. The goal of this densification was to monitor the intended small scale injection test and acid stimulation in the geothermal well with improved sensitivity and precision. Following other similar projects the response of the subsurface to this injection test was expected to be benign. The recorded micro-earthquakes were intended to be used to improve our understanding of the geothermal system and the subsurface in addition to calibrate statistical earthquake models for the development of an ATLS (e.g. Gischtig & Wiemer 2013). After the induced $M_L = 3.5 \pm 0.1$ earthquake on July 20 the mobile network was further densified by three short-period stations (SGT[10–12] blue circles in Fig. 1). Between then and May 2014, when the mobile network was dismantled, part of the network was upgraded to include solar power and mobile communications. As a result, some of the stations had to be slightly relocated (re-named SGT[13–17]) to adapt to the new conditions imposed by this hardware. In total the mobile network occupied 11 different sites, with a maximum of seven stations running at any one time.

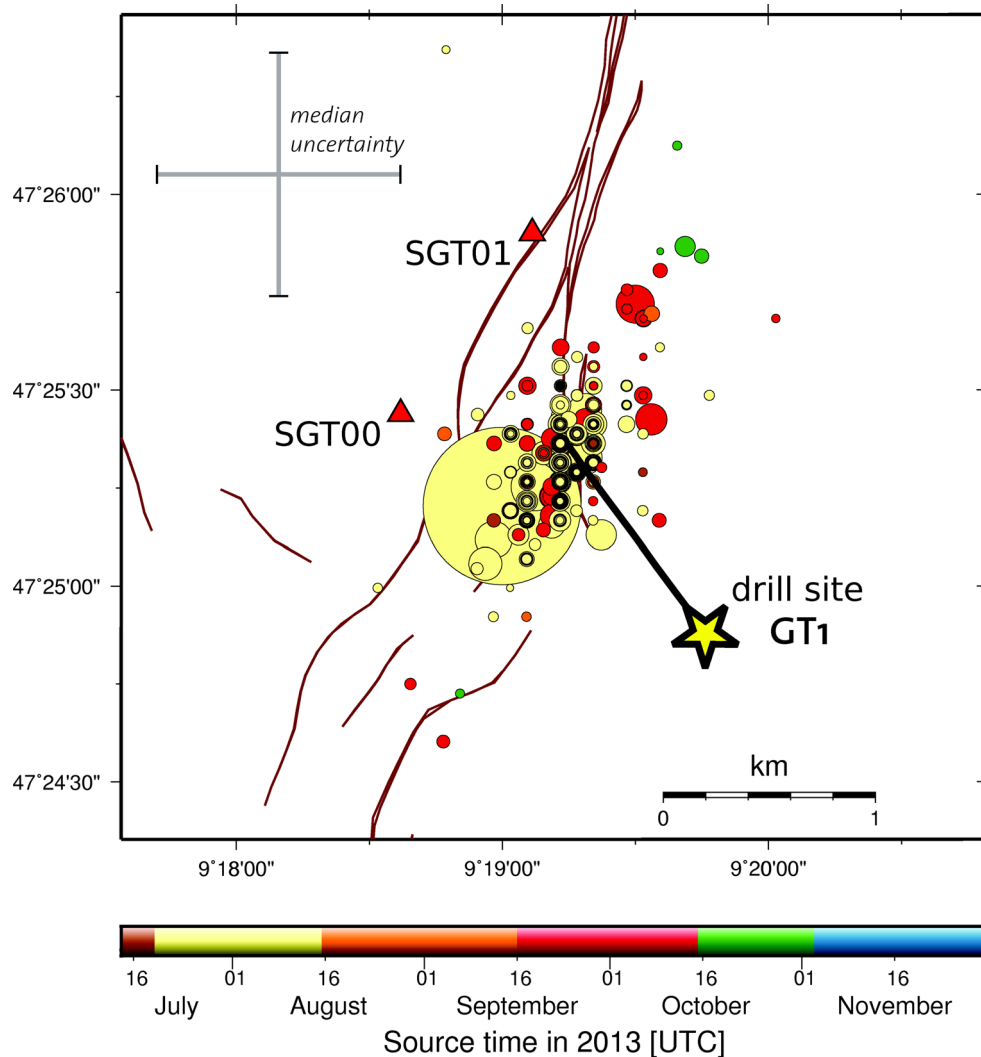


Figure 2. Map of routine analysis earthquake locations. Size of circles corresponds to Brune source radius assuming a stress drop of 0.1 MPa (Bay *et al.* 2005; Edwards & Fäh 2013). Median location uncertainty is indicated in the upper left-hand corner. Colour code indicates the source time of the events. The St Gallen Fault Zone as derived from 3-D seismics, which was reactivated by the injection is indicated as red lines.

EARTHQUAKE LOCATIONS

Earthquake locations were derived in the framework of the routine earthquake analysis at the SED (Fig. 2). Events down to magnitude $M_{L,corr} = 0.3$ (see section ‘Station Corrections for the Local Monitoring Network’) were detected automatically by the SED analysis system (SeisComp3; Hanka *et al.* 2010; Diehl *et al.* 2013). Events with magnitudes smaller than this threshold were identified by daily manual screening of the data recorded by the borehole station (SGT00). In total 864 seismic events were detected between 2013 July 14 and December 18. Of these events 349 were strong enough to be located using a fully probabilistic non-linearized inversion approach (NonLinLoc, Lomax *et al.* 2000) and a 3-D seismic velocity model (Husen *et al.* 2003). The earthquake locations have a median uncertainty of ± 0.6 km horizontally and ± 1.2 km in depth. A subsequent double-difference (DD) relative relocation took advantage of highly accurate relative arrival times derived from cross-correlation, and reduced these uncertainties by nearly two orders of magnitude (Diehl *et al.* 2014). Stringent quality control slightly reduced the number of earthquakes in the data set of Diehl *et al.* (2014). As the absolute locations of the NonLinLoc analysis do not

differ substantially from the overall DD results, we use the more complete NonLinLoc result in this study.

EARTHQUAKE MAGNITUDES

Earthquake magnitudes are often determined from either band-limited single point measures of a seismogram (e.g. the local magnitude: M_L , Richter (1935)) or from broad-band signals (e.g. moment magnitude: M_w , Hanks & Kanamori (1979)). Different magnitude scales reflect different source properties or combinations thereof (e.g. duration, slip area, stress-drop Hanks & Boore 1984), and subsequently one event can have numerous magnitudes assigned to it. Common to all magnitude classifications is the correction for attenuation: as seismic waves propagate through the Earth, they lose energy due to both intrinsic (e.g. frictional) and non-intrinsic (e.g. geometrical) effects. Recorded seismograms are therefore corrected to provide the earthquake’s magnitude at a common reference distance. It is principally this correction, typically empirically derived, which is subject to non-uniqueness. As a result, a single earthquake

may be assigned different magnitudes (of the same type) depending on the procedures of the network operator (e.g. Fäh *et al.* 2011).

In addition to the ambiguity arising from the attenuation correction of recorded seismograms, the radiation pattern and local site effects (Steidl *et al.* 1996), as well as true aleatory variability lead to different magnitudes being assigned to one event by two stations, even if they are at the same distance from the source. Site effects are primarily due to the interaction of the wavefield with the upper-most layers of the Earth: soil and weathered rock. The resulting resonance, focussing or defocussing, and attenuation can lead to ground motion amplification factors of up to ten or more between sites which are only a few hundred metres apart, yet have starkly different local geology. Typically, modern seismic observatories aim to install national monitoring networks on rock sites, where site amplification is less of an issue. Averaging out effects over several stations with a range of distances (and corresponding attenuation corrections) means that magnitudes of earthquakes $M > 2$ are generally robust. High quality broad-band seismometers located in areas with very low background noise are even able to locate very small events at significant distances (e.g. station FIESA of the SDSNet can record events of $M_L = -0.5$ at up to 45 km distance). However, in general, as earthquake sizes decrease, given uniform background noise, smaller and smaller interstation spacing and higher quality instrumentation are required in order to record seismograms above the noise level. This means that in practice, where micro-earthquakes are expected, local monitoring networks are established with station spacing on the order of a few kilometres. Whilst this ensures that earthquakes are reliably recorded, it unfortunately leaves the subsequent interpretation in terms of magnitude susceptible to problems. First, and perhaps counter intuitively, the limited distance range at which recordings are made means that attenuation correction bias can have a big impact: since attenuation relations are typically calibrated from distances greater than tens of km, the correction is not necessarily valid. Secondly, local networks cannot be established exclusively on rock sites: site amplification, reflective of local soils and geology, can therefore lead to systematic bias. While reducing the interstation spacing and instrument quality can help to record smaller and smaller events, the background microseism also presents an effective noise floor, with corresponding minimum recordable magnitude. The only way to avoid this is to install borehole instrumentation. Due to high costs, the number of boreholes is often minimized: that is, in the case of St Gallen to one. Determining reliable (robust) magnitudes on a single borehole station is explored in the section ‘Station Corrections for the Local Monitoring Network’.

St GALLEN MAIN SHOCK MAGNITUDE

The local magnitude scale used by the SED is based on a modification (Kradolfer 1984) of the original formulation of Richter’s (1935) local magnitude scale:

$$M_L(\text{SED}) = \log A_0 + C_d + C_e \quad (1)$$

with A_0 the maximum mean-to-peak horizontal amplitude in mm on a 2800× Wood-Anderson torsion seismometer [SED does not use the ×2080 correction of Uhrhammer & Collins (1990)]. C_d is a distance correction, given by:

$$\begin{aligned} C_d &= 0.0180 R + 1.77 & \text{for } R \leq 60 \text{ km} \\ C_d &= 0.0038 R + 2.62 & \text{for } R > 60 \text{ km} \end{aligned} \quad (2)$$

with R the hypocentral distance in kilometres. This scaling relation was derived using vertical recordings on short-period instrumentation with analogue telemetry. $C_e = 0.1$ is an empirically derived correction to the scaling relation that was implemented to maintain consistency in the M_L (SED) scale after the upgrade to a fully digital three-channel broad-band network. Interestingly the attenuation correction lacks a $\log(R)$ term, typically used to account for geometrical spreading (e.g. Dost *et al.* 2004). We later see that this has a significant impact in the first 20 km: a distance range not considered during the model’s development due to the much larger interstation spacing present in 1984.

The main shock of the St Gallen Project was manually located and assigned $M_L = 3.5 \pm 0.1$, using only broad-band SDSNet stations at $R > 20$ km (excluding strong-motion instruments, which are often located on strongly amplifying soils). Fig. 3 shows M_L computed for each station of the network. The amplification present at some strong motion sites (not used for the average) and the strong distance dependent trend at $R < 20$ km are clearly apparent.

Immediately from Fig. 3 we can observe the problem for determining the magnitudes of smaller events: as their size decreases, the availability of broad-band station recordings at $R > 20$ km will diminish. For the smallest events recorded only on the local network, we will be inside the region of biased attenuation correction, and in addition, potentially subject to systematic local amplification effects.

STATION CORRECTIONS FOR THE LOCAL MONITORING NETWORK

It is difficult to separate the effects of attenuation and site amplification in the case of few recordings. However, the fact that all the events related to the geothermal project were concentrated in a relatively small area means that the source-station distances, particularly after considering location error, are almost constant. It was therefore decided as an intermediate solution to search for site-specific distance independent M_L corrections. These corrections account for both the bias of the attenuation correction at $R < 20$ km and any potential site amplification effects (Fig. 4).

The site specific corrections ($\Delta M_{L,\text{stn}}$) were determined by using a set of reference events (Table 1): those large enough to be recorded and assigned M_L on the distant ($R > 20$ km) broad-band stations of the SDSNet. By then computing station specific magnitudes on the local monitoring network ($M_{L,\text{stn}}$) and averaging the residuals ($M_{L,\text{stn}} - M_L$) over N available events and we obtained the corrections (Fig. 5, Table 1):

$$\Delta M_{L,\text{stn}} = -\frac{1}{N} \sum_{\text{stn}=1}^N (M_{L,\text{stn}} - M_L). \quad (3)$$

Applying the station corrections in Fig. 5 ($M_{L,\text{corr,stn}} = M_{L,\text{stn}} + \Delta M_{L,\text{stn}}$) and taking the median value over all stations we refer to the scale $M_{L,\text{corr}}(\text{SED})$, or for brevity $M_{L,\text{corr}}$. The two groups of corrections (approximately -1.0 to -1.2 and -0.2 to -0.4) correspond to the inner and outer ring of the network, respectively. The primary influence to the correction terms is clearly the attenuation correction bias.

The smallest events ($M_L < -1$) are only detected on the central borehole station of the St Gallen monitoring network. To be able to determine magnitudes for these small non-locatable events, we compare $M_{L,\text{corr}}$ of the larger events to the logarithm of the maximum ground motion amplitude (A) observed at the borehole station. We

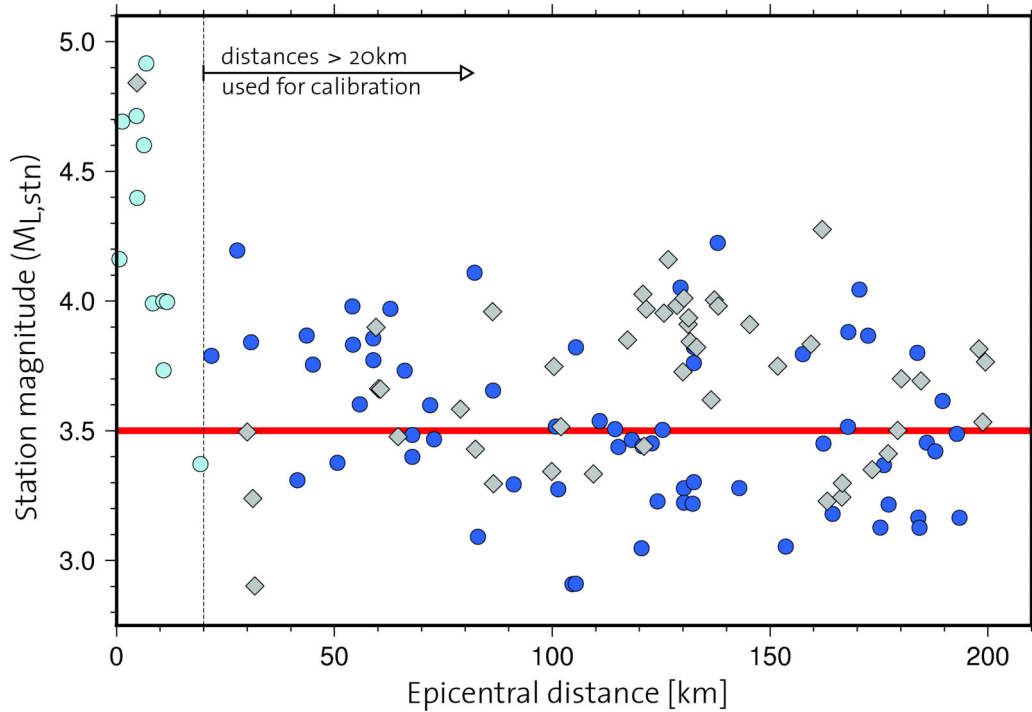


Figure 3. Plot of station specific M_L versus distance for the 2013 July 20 St Gallen main shock ($M_L = 3.5$). Broad-band stations (blue circles) with $R > 20$ km were used for the average magnitude determination. The median of the station magnitudes used ($M_L = 3.5$) is indicated by a red line. Strong motion stations (grey diamonds) and stations with $R < 20$ km are excluded from the calibration.

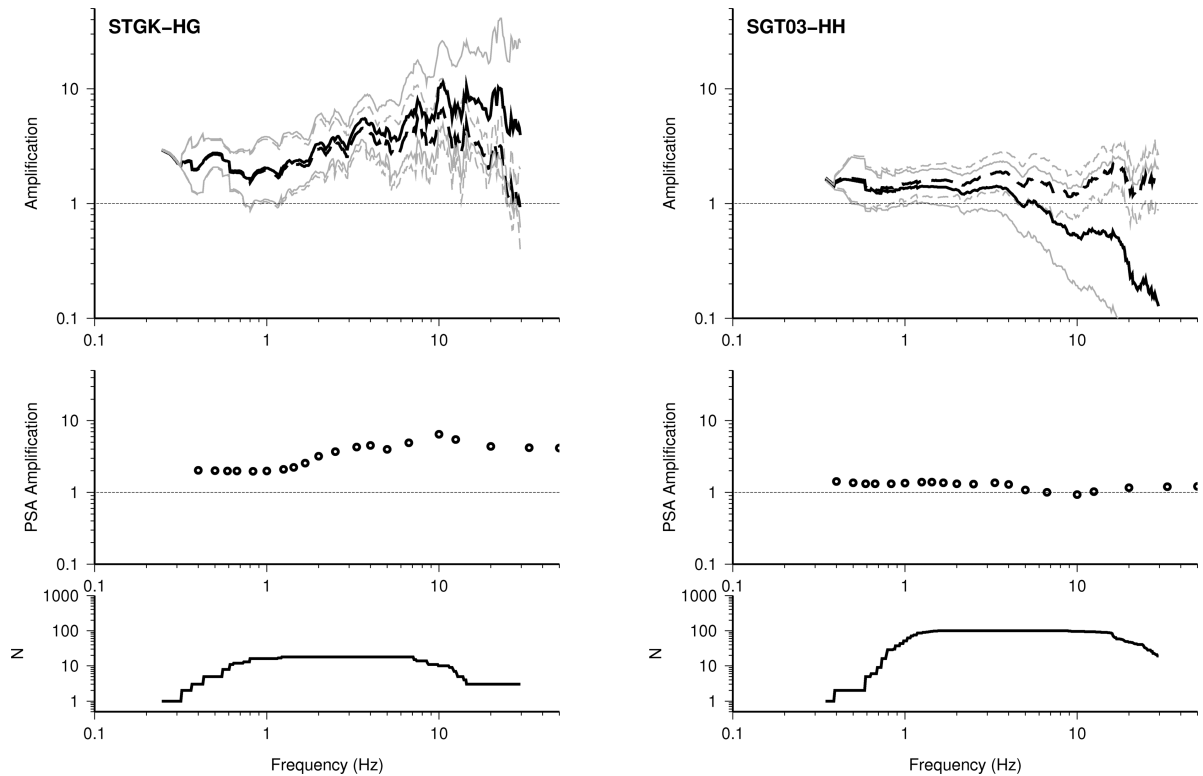


Figure 4. Strongly (left, site STGK) and weakly- or non-amplifying (right, site SGT03) sites of the local monitoring network. Top panel: Fourier amplification relative to the Swiss reference rock model (Edwards *et al.* 2011; Poggi *et al.* 2011) (solid black line: elastic, dashed black line: anelastic, grey lines: uncertainty). Middle panel: 5 per cent damped pseudo-spectral acceleration amplification. Bottom panel: number of recordings.

Table 1. Reference events with M_L determined only at $R > 20$ km and on SDSNet stations.

Date	Time	M_L
2013 July 19	18:51:56	1.48
2013 July 20	00:14:28	1.63
2013 July 20	00:40:40	2.08
2013 July 20	03:30:54	3.50
2013 July 20	03:41:47	1.29
2013 July 20	13:45:29	1.69
2013 July 21	05:14:16	1.14
2013 July 23	08:58:54	1.81

calculated A as the maximum of the quadratic mean over the three orthogonal sensor components:

$$A = \max\left(\sqrt{X^2 + Y^2 + Z^2}\right) \quad (4)$$

in a 1.7 s long time window including P and S onset, bandpass filtered between 10 and 40 Hz. As can be seen in Fig. 6, $\log_{10}(A)$ and $M_{L,corr}$ correlate very well with a small standard deviation of 0.17. A linear regression analysis resulted in the relationship:

$$M_{L,corr} = [1.02 \log_{10}(A) - 0.67] \pm 0.17. \quad (5)$$

This result indicates that for the St Gallen sequence reliable estimates of $M_{L,corr}$ can be derived from observations at a single station.

SEPARATING ATTENUATION AND AMPLIFICATION EFFECTS

The scheme detailed in the previous section allows the unbiased estimation of M_L for small events in a given source region using only recordings of the local monitoring network. Such an approach can easily be applied as long as wider regional seismic network exists and there have been a few events with $M \gtrsim 1.5$ (depending on the network sensitivity). From the previous analysis it is obvious that there is a fundamental problem with the SED attenuation correction (eq. 2) at $R < 20$ km. In order to address this issue, we collected station magnitudes ($M_{L,stm}$) ($0 < R_{epi} < 500$ km) from 2693 Swiss or border region earthquakes with magnitudes $0 > M_L > 5$. It should be noted that for computing event M_L , station magnitudes at $R < 20$ km have never been used: catalogue magnitudes are therefore unaffected by this issue. At distances greater than 20 km the residual $M_{L,stm} - M_L$ has zero mean, showing that the attenuation correction is suitable within the range of distances used in its derivation (Kradolfer 1984). However, for distances below 20 km there is a significant trend in the station magnitude residual that is similar to that observed for the St Gallen earthquake. A complete renewal of the attenuation correction at all distances would be one solution to this issue. However, since the attenuation correction for $R > 20$ km works, and the fact that existing earthquake magnitudes were only calculated using stations at distances greater than 20 km, we can simply add an additional attenuation correction for the case $R < 20$ km. This approach then has a significant advantage that it will not affect the existing earthquake catalogue (ECOS09).

Since most recordings are from small events there is a risk that localized site effects could bias the observed attenuation in the near-field. Site specific M_L corrections were therefore determined from the broad-band amplification functions routinely determined for the stations of the seismic network (Edwards *et al.* 2013) using a random-vibration theory approach (Hanks & Boore 1984). After

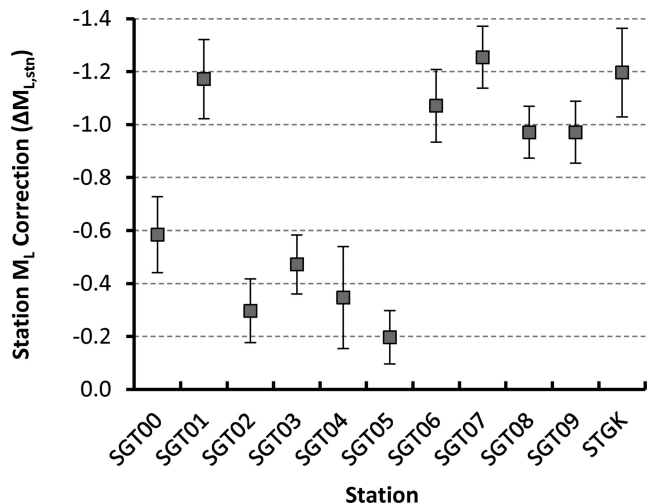


Figure 5. Station M_L correction ($\Delta M_{L,stm}$) and standard-deviation over the eight calibration events for the 11 stations of the local monitoring network.

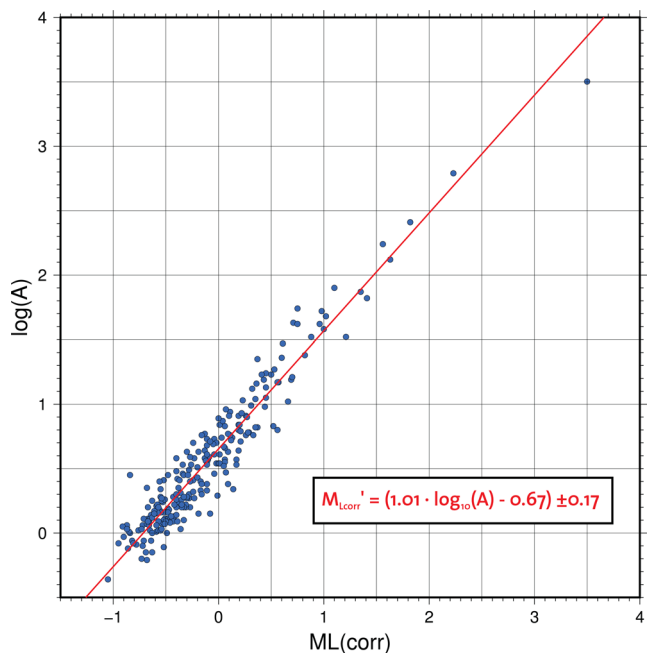


Figure 6. Comparison of station corrected event magnitude $M_{L,corr}$ and the logarithm of the maximum ground motion amplitude observed at the borehole station SGT00 [$\log(A)$]. Red line indicates the result of the linear regression.

correction of the station magnitudes, the event M_L was recomputed using only data with $R > 20$ km. The resulting station magnitude residuals are plotted in Fig. 7. We determined the attenuation correction using a least-squares fit to the site amplification corrected $M_{L,stm} - M_L$ residuals as a function of $\log_{10}(R/20)$, forcing the intercept to zero. This defines that the correction is zero at 20 km. The resulting modified attenuation correction for the M_L scale is:

$$\begin{aligned} C_d &= 0.0180 R + 1.77 + 0.968 \log_{10}(R/20) \quad \text{for } R \leq 20 \text{ km} \\ C_d &= 0.0180 R + 1.77 \quad \text{for } R \leq 60 \text{ km} \\ C_d &= 0.0038 R + 2.62 \quad \text{for } R > 60 \text{ km} \end{aligned} \quad (6)$$

with R the hypocentral distance in km. This results in zero mean and no trend in the station magnitude residuals from zero to 500 km. The

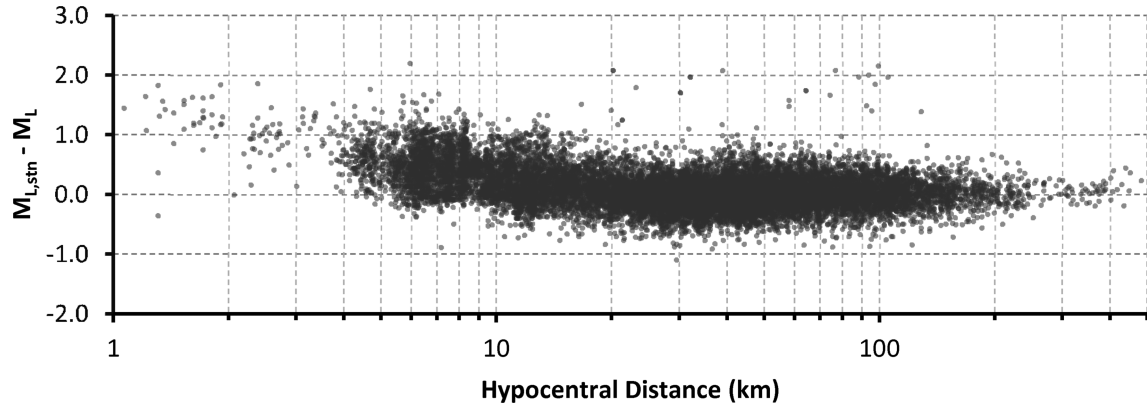


Figure 7. Station magnitude residuals $M_{L,stm} - M_L$ (corrected for amplification, but not the incorrect near-source attenuation) plotted against hypocentral distance.

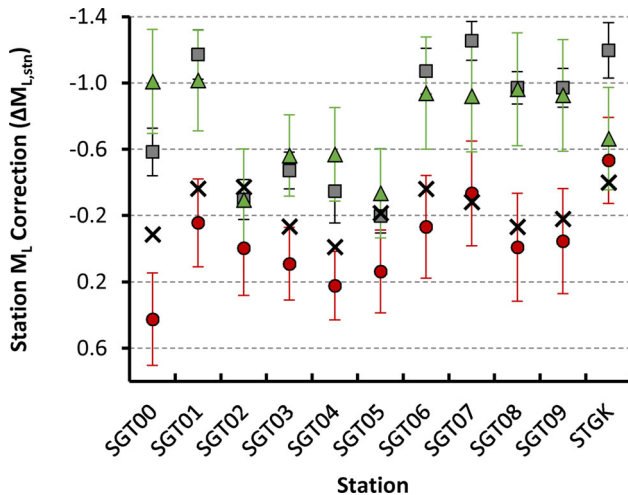


Figure 8. As Fig. 5, with the station correction terms ($\Delta M_{L,stm}$) calculated using the new attenuation correction (eq. 6, circles). In addition the contribution to the site terms from the incorrect attenuation function is shown (triangles). The mean amplification correction based on independent broadband site-amplification functions are shown as crosses. A negative correction indicates sites exhibiting amplification and vice versa.

form of the correction below 20 km implies geometrical decay with $R^{-0.97}$. However, physical interpretation of this should consider the strong trade-off between intrinsic and geometrical attenuation. For example, we note that while geometrical attenuation obviously still occurs at distances greater than 20 km, a $\log(R)$ term—associated to geometrical decay—is not required in the attenuation correction at these distances. Using the new attenuation correction we are able to determine the component of the site-correction terms that are due to site amplification (Fig. 8). Comparing these values to those based on the independently derived broadband site amplification functions (e.g. Fig. 4), we see that the values are generally within one sigma, apart from at the borehole station (SGT00).

MOMENT MAGNITUDE DETERMINATION

The moment magnitude of small events can be determined from the long-period plateau of the Fourier displacement spectrum (e.g. Scherbaum 1990; Ottemoller & Havskov 2003). We used the spectral M_w determination method of Edwards *et al.* (2010). The method

models recorded earthquake spectra using the far-field instantaneous slip model of Brune (1970), which related the long-period plateau of the Fourier displacement spectrum to the seismic moment. In order to provide robust solutions for small and moderate earthquakes, typically recorded at distant instruments with limited bandwidth remaining, corrections for intrinsic attenuation are applied (in the case of Edwards *et al.* 2010 as part of the minimization). Edwards *et al.* (2010) showed that their method provided 1:1 conformity to available moment tensor solutions in Switzerland with an uncertainty of approximately 0.1. Their method, among two others, was applied to events in Switzerland with $M_L \geq 1.5$ for the determination of a M_L to M_w conversion relation (Goertz-Allmann *et al.* 2011) which is also consistent with other European relations (Grünthal *et al.* 2009).

Since the small shocks studied here typically have a strongly limited bandwidths, but are small enough that their source corner-frequency is above 10 Hz, we can assume that the Fourier displacement spectrum is simply flat up to 10 Hz. Initially, all spectra were checked for their signal-to-noise ratio (SNR) to avoid any possible noise contamination. All spectra with a SNR > 1.5 at 8–9 Hz were then selected. We fit the model between their minimum and maximum frequencies with SNR > 1.5, limiting the upper bound to 10 Hz. The spectral plateau values were then corrected for geometric attenuation ($1/R^{1.3}$; Edwards & Fäh 2013), and a simultaneous inversion was performed to separate the average site amplification and moment magnitude. In order to constrain the inversion, we fixed the amplification of SGT03 (Fig. 4) to unity, as this was determined separately to the studied sequence (Edwards *et al.* 2013).

The resulting M_w are compared with M_L with and without correction terms ($\Delta M_{L,stm}$) in Fig. 9. Since the catalogue M_L magnitudes are based on the old attenuation correction we had to use the correction that accounts for both site amplification and the attenuation correction bias at the station-seismic cloud distance. In both cases, the larger events are unaffected by the use of the station corrections, since they were robustly determined initially. In the case of the corrected $M_{L,corr}$ (Fig. 9b), the M_L : M_w values follow a linear trend. As found for a variety of regions (Edwards & Douglas 2014) the form of this trend above $M_L \approx 1$ is almost exactly that defined by Goertz-Allmann *et al.* (2011). Comparing the uncorrected M_L values, the trend clearly breaks down as values fall below $M_L \approx 1$: the point at which the local network is used exclusively to define the magnitude. On the other hand, the station-corrected values ($M_{L,corr}$) continue the trend below $M_L \approx 1$, although leading to slightly lower M_w than predicted by the Swiss M_L : M_w of

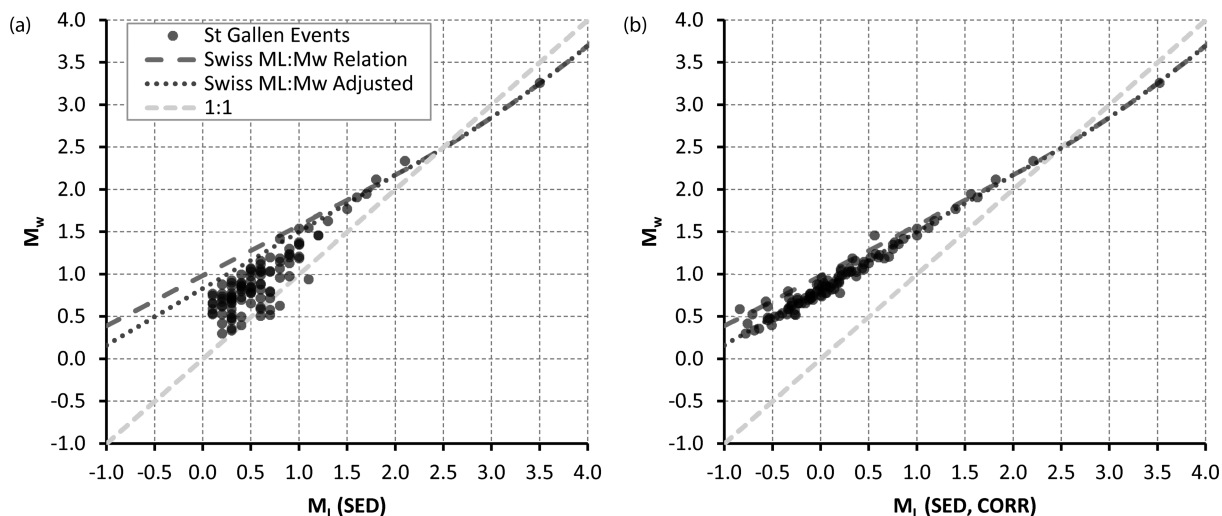


Figure 9. M_w plotted against M_L using (a) uncorrected M_L and (b) $M_{L,corr}$ corrected using station terms. M_L : M_w scaling relations of Goertz-Allmann *et al.* (2011) and the adjusted relation in eq. (7) are shown.

Goertz-Allmann *et al.* (2011). Bethmann *et al.* (2011) empirically found that M_w scales proportional to $0.67 M_L$ for very small earthquakes in Switzerland. This is consistent with theoretical arguments (Deichmann 2006) and the result of simulations (Hanks & Boore 1984; Edwards *et al.* 2010), with the explanation being that near-surface attenuation imposes a minimum limit to the observed pulse duration: such that $M_L \propto M_0$ and therefore $M_L \propto 2/3 M_w$. Modifying the Goertz-Allmann *et al.* (2011) relation for this, we see an almost perfect conformity to the measured values in St Gallen. The scaling relation of Goertz-Allmann *et al.* (2011), including modification to the part with $M_L < 2$ is then:

$$\begin{aligned}
 M_w &= (2/3)M_L + 0.833 & M_L < 2 \\
 M_w &= 1.327 + 0.253 \times M_L + 0.085 \times M_L^2 & 2 \leq M_L \leq 4 \\
 M_w &= M_L - 0.3 & M_L > 4
 \end{aligned} \tag{7}$$

COMPARISON BETWEEN TWO $M_L \approx 3.5$ INDUCED EVENTS: St GALLEN AND BASEL

Instrumental ground motion

In 2006, prior to the St Gallen deep geothermal project, an EGS project in Basel, Switzerland, took place. The Basel project was ultimately cancelled after an $M_L = 3.4 \pm 0.1$ ($M_w = 3.2 \pm 0.1$) event was triggered, causing widespread minor (non-structural) damage (Giardini 2009). Despite the slightly greater magnitude of the St Gallen event, and despite also being widely felt, little damage was reported. To put the exposure in context, according to the Swiss Federal Statistical Office, the population density in Basel is 6900 km^{-2} , while in St Gallen it is 1900 km^{-2} . Both the Basel 2006 ($M_w = 3.2 \pm 0.1$; $M_L = 3.4 \pm 0.1$) and the St Gallen 2013 ($M_w = 3.4 \pm 0.1$; $M_L = 3.5 \pm 0.1$) events were clearly recorded by the continuous broad-band and strong-motion seismic stations monitored by the SED. The typical SED modern seismic station consists of either a STS-2 (or Trillium Compact) broad-band sensor or a strong-motion EpiSensor ES-T continuously recording on 24-bit digitizers. The Basel earthquake also triggered several low-gain strong-motion stations installed in the mid-1990s (typically equipped with 12-bit and 16-bit digitizers) and still operating in the epicentral area at the

time of the event. Fig. 10 shows the geometric mean of horizontal components for available peak-motions [peak ground velocity (PGV), and peak ground acceleration (PGA)] and 5 per cent damped pseudo-acceleration (PSA) at vibration periods $T = 0.3 \text{ s}$ and $T = 1 \text{ s}$ as function of the distance from the hypocentre. All raw waveforms were uniformly resituated to ground-motion and bandpass filtered using a fourth-order acausal Butterworth with low-cut at 0.33 Hz . As expected based on the similar magnitude and depth of the causative events, on a logarithmic scale peak-motions and response spectral amplitudes are fairly comparable (Fig. 10). The strongest shaking was observed in both cases in the epicentral region, with PGV values approaching $1\text{--}2 \text{ cm s}^{-1}$ and PGA reaching 0.1 g . These ground-motions are around the threshold at which damage is expected to occur (Worden *et al.* 2012). Median attenuation curves predicted by the Swiss stochastic model of Edwards & Fäh (2013) as parametrized by Cauzzi *et al.* (2015) are shown in Fig. 10. The black and red curves in each panel represent the median predictions for a $M_w = 3.2$ (Basel) and $M_w = 3.4$ (St Gallen) earthquake in the Swiss foreland (EF13_f). Since data shown in Fig. 10 were not segregated into different soil classes or ground types, the hard-rock (i.e. $V_{S30} \approx 1100 \text{ m s}^{-1}$) predictions of Edwards & Fäh (2013) were modified to take into account an average amplification to generic rock-like conditions (i.e. $V_{S30} \approx 620 \text{ m s}^{-1}$) based on the Swiss macroseismic intensity catalogue (Fäh *et al.* 2011), as described in Cauzzi *et al.* (2015). Even so, the data recorded in the near-epicentral region systematically exceed the median values predicted by the Swiss stochastic model. This is due to the combined effect of the shallowness of the event and the significant effect of local amplification, particularly at the recording sites in the epicentral region, reaching, for example factor ~ 6 in Basel and ~ 3 in St Gallen for PGV with respect to the Swiss reference rock (Poggi *et al.* 2011; Edwards *et al.* 2013). In addition to local amplification effects, Atkinson (2015) showed that the rate of geometrical attenuation has a significant effect on ground-motions in the near-field. This may indicate that for these events attenuation may be even stronger than the $R^{-1.3}$ used in the predictive model.

In Fig. 10, we observe that for long period (1 s) PSA is, on average, systematically slightly higher in the case of St Gallen due to its higher M_w . At shorter periods the ground motions of the two events are, over the range of recording distances, comparable. In fact the distinction between the two GMPE curves (different due

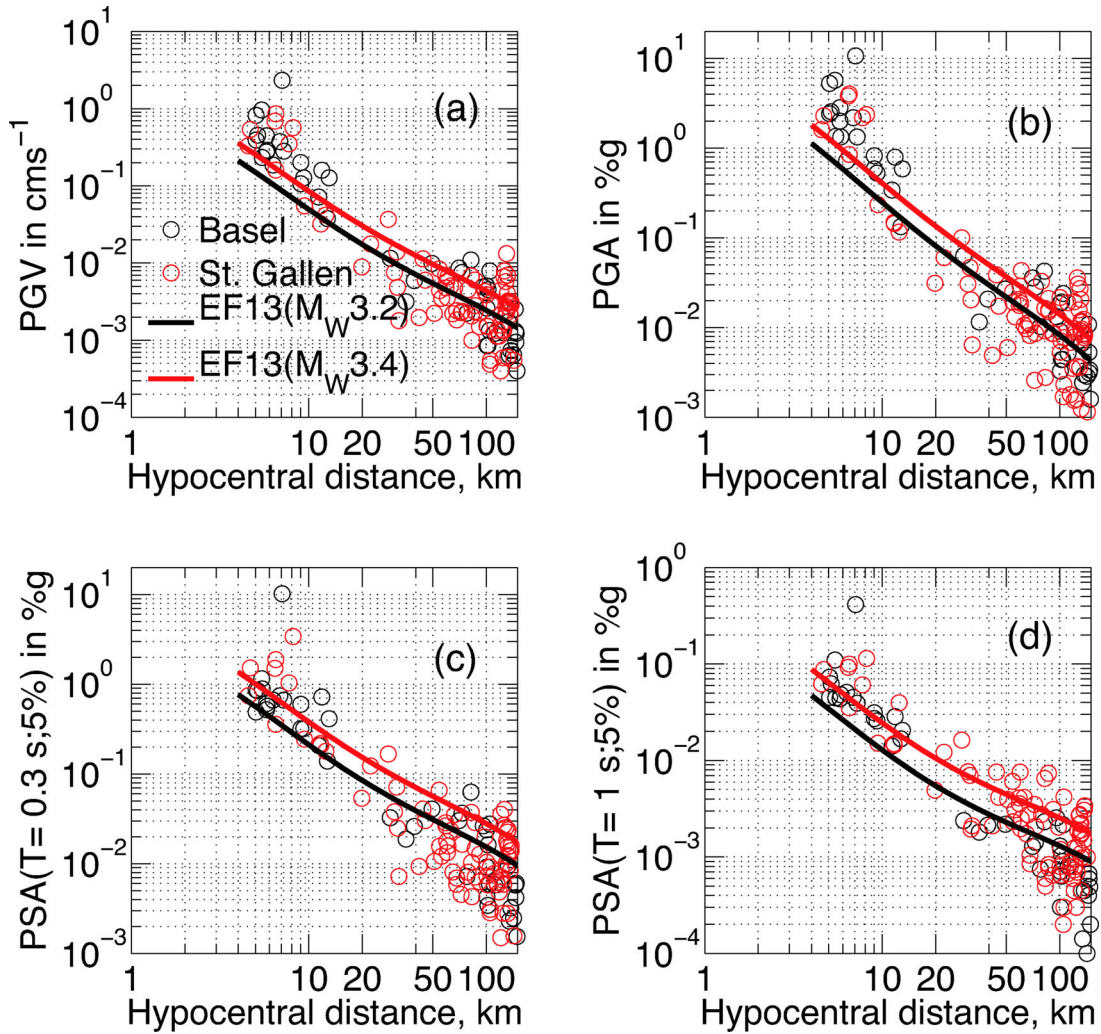


Figure 10. Attenuation of PGV (a), PGA (b) and 5 per cent-damped PSA ($T = 0.3$ s) (c) and PSA ($T = 1$ s) (d), as a function of hypocentral distance. Black circles show peak motion and spectral data for the Basel 2006 $M_w = 3.2$ event. Red circles refer to the St Gallen 2013 $M_w = 3.4$ event. EF13 is the median attenuation curve for events occurring in the Swiss foreland (Edwards & Fäh 2013; Cauzzi *et al.* 2015), computed as explained in the text.

to the different input M_w values) at high frequency (Fig. 10b) is not observed in the data. One hypothesis for this observation would be that despite the lower M_w value of the Basel event, more high frequency energy was radiated (with respect to that expected for a given M_w event). This should manifest as higher stress-parameter for the Basel event (Edwards *et al.* 2010), and thus a similar M_L should be expected for the two events. These observations are consistent with the published magnitudes, with 0.2 units difference observed between M_w and 0.1 units in M_L .

Whilst average ground-motion is important to seismologically characterize events, analysis of site-specific recordings can give an insight into localized effects that may impact macroseismic observations or even damage in the epicentral region. Fig. 11 shows the largest 5 per cent-damped elastic response spectra (geometric mean of the horizontal components) computed from the available waveforms in the epicentral region. In the case of Basel, this recording, compared to others at similar distances, reached exceptional levels. Pseudo-acceleration (PSA) spectra are given in Fig. 11(a), while Fig. 11(b) shows displacement response spectra (DRS) to emphasize the relevant features of the seismic demands at intermediate vibration periods. The largest spectral amplitudes were observed at station SBEG and STGK, for the Basel and St Gallen events,

respectively. The stations are located at comparable epicentral distances (~ 5 km) and pertain to the same Eurocode 8 (CEN 2004) ground type B (i.e. $V_{S30} \approx 440$ m s $^{-1}$). They exhibit strong average PSA amplification (Fig. 11c) relative to the reference rock model of Poggi *et al.* (2011), reaching peak levels of factors 4.9 (SBEG, Basel) and 7.3 (STGK, St Gallen; Michel *et al.* 2014). Despite this, the spectral levels at SBEG (Basel) are remarkably higher than those observed at STGK (St Gallen), with a dominant PSA peak exceeding 0.3 g at ~ 0.08 s. It should be noted that such differences are not necessarily unusual: the aleatory component of ground motion variability is typically around a factor 2 at one sigma. However, also notable at SBEG (Basel) are the spectral peaks apparent for $0.1 < T < 0.3$ s, exceeding 0.3 g and 0.2 cm within the typical vibration period range of low-rise buildings.

Macroseismic intensity

Fig. 12 shows the SED ShakeMaps (USGS code version 3.5; Wald *et al.* 1999, 2005; Worden *et al.* 2010) for the Basel 2006 ($M_w = 3.2$) and the St Gallen 2013 ($M_w = 3.4$) events.

Colours are proportional to EMS-98 intensity levels (Grunthal 1998; Grünthal *et al.* 2001), computed using: (i) the

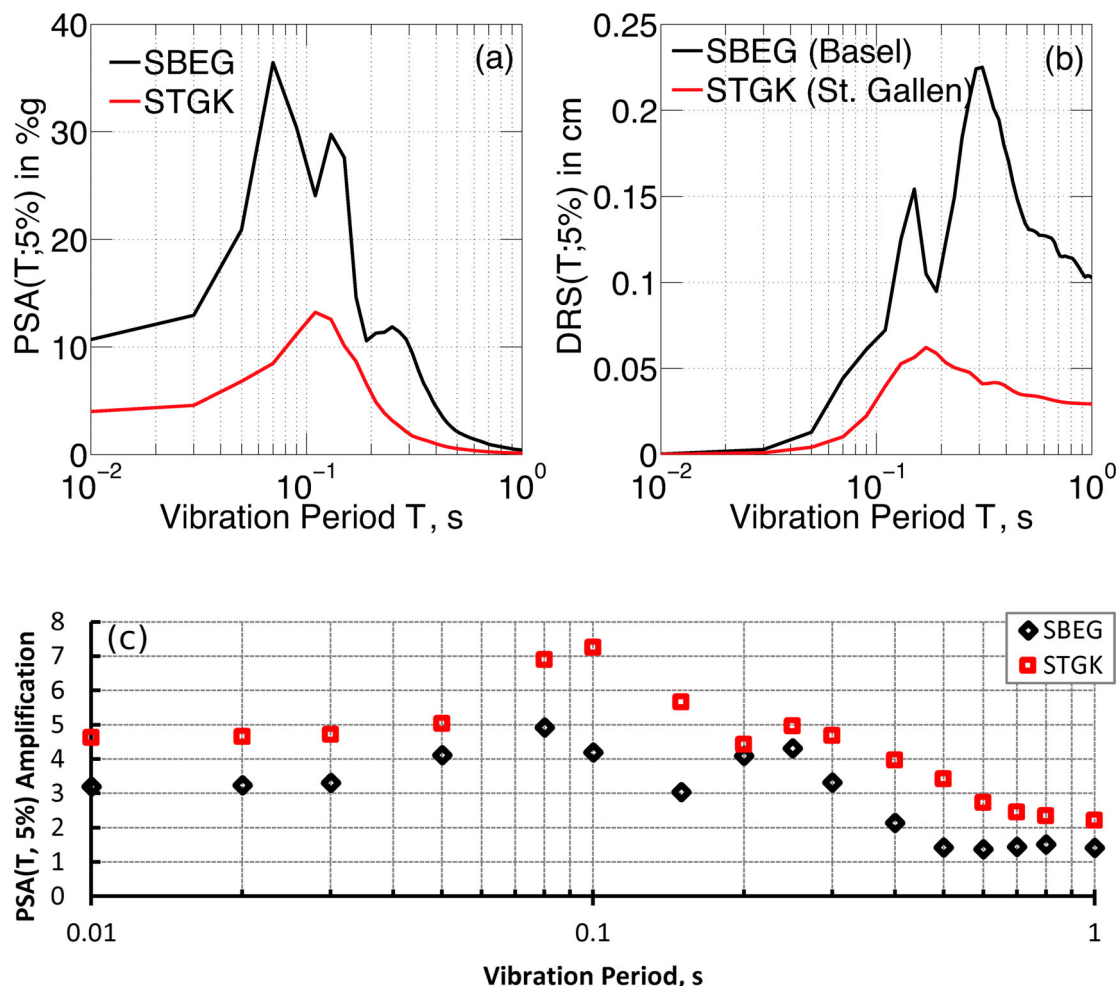


Figure 11. Top panel: largest 5 per cent-damped PSA spectra and DRS (geometric mean of the horizontal components) observed for (a) the Basel 2006 M_w 3.2 event at stations SBEG and (b) the St Gallen 2013 M_w 3.4 earthquake at station STGK. (c) PSA amplification at sites SBEG and SGTK. Red lines and symbols refer to St Gallen and black to Basel.

parametrization of the semi-stochastic ground-motion prediction model at hard rock sites by Edwards & Fäh (2013) (see Cauzzi *et al.* 2015); (ii) the ground-motion to intensity conversion equation (GMICE) of Faenza & Michelini (2010); (iii) the regional amplification factors based on macroseismic intensity data of Kästli & Fäh (2006) and Fäh *et al.* (2011). For each recording station (triangles in Fig. 12), the peak-motion parametric data to be used as input to *ShakeMap* were computed using the SeisComp3 (Hanka *et al.* 2010) software module *scwfparam* (Cauzzi *et al.* 2013) and the amplification factors (in terms of macroseismic intensity) were replaced by the empirical amplification (recorded over numerous previous events) with respect to the Swiss reference rock model of Poggi *et al.* (2011). The reader is referred to Cauzzi *et al.* (2015) for further details about SED ShakeMap implementation. Consistent with near source PGV values of $\sim 1\text{--}2\text{ cm s}^{-1}$ and the use of the GMICE by Faenza & Michelini (2010), both ShakeMaps show macroseismic intensity levels approaching degree V in the epicentral area. While epicentral intensity V is the same level attributed to the Basel 2006 event in the recently compiled earthquake catalogue of Switzerland (ECOS-09; Fäh *et al.* 2011), analysis of the felt reports of the St Gallen 2013 event suggest an intensity of IV in the epicentral area.

The macroseismic intensity of the St Gallen earthquake was assessed using a standard ‘Felt Reports’ procedure implemented at the SED. A questionnaire was requested from the general public.

The content of the questionnaire, which has not been changed since 1999, describes earthquake effects both with multiple choice questions and free text. Responses were collected in three ways:

- (1) The questionnaire was offered to people visiting the SED website to look for earthquake information. This sample is typically biased towards people who have felt an earthquake themselves.
- (2) Roughly 2500 interested people in the potentially affected area who were subscribed to a mailing list were contacted by email, with the request to describe their observations (independent of whether they had felt the earthquake or not).
- (3) Paper questionnaires were sent to public institutions, such as post offices, municipal administrations, restaurants, etc. for further distribution.

For the main shock related to the St Gallen geothermal project, we collected 429 interpretable questionnaires, of which 378 report to have felt the earthquake, with the remaining 51 saying that the earthquake was not felt. Intensities were assessed per postcode area, first applying a standardized algorithm to attribute a raw intensity. The raw intensity is manually reviewed and checked for consistency with the effects from text descriptions in the questionnaire. Based on this data, a high-quality intensity could be assessed for 23 postcode areas (Fig. 13). All assessed intensities were IV on EMS scale. For many other sites, only few (typically <5), or rather heterogeneous

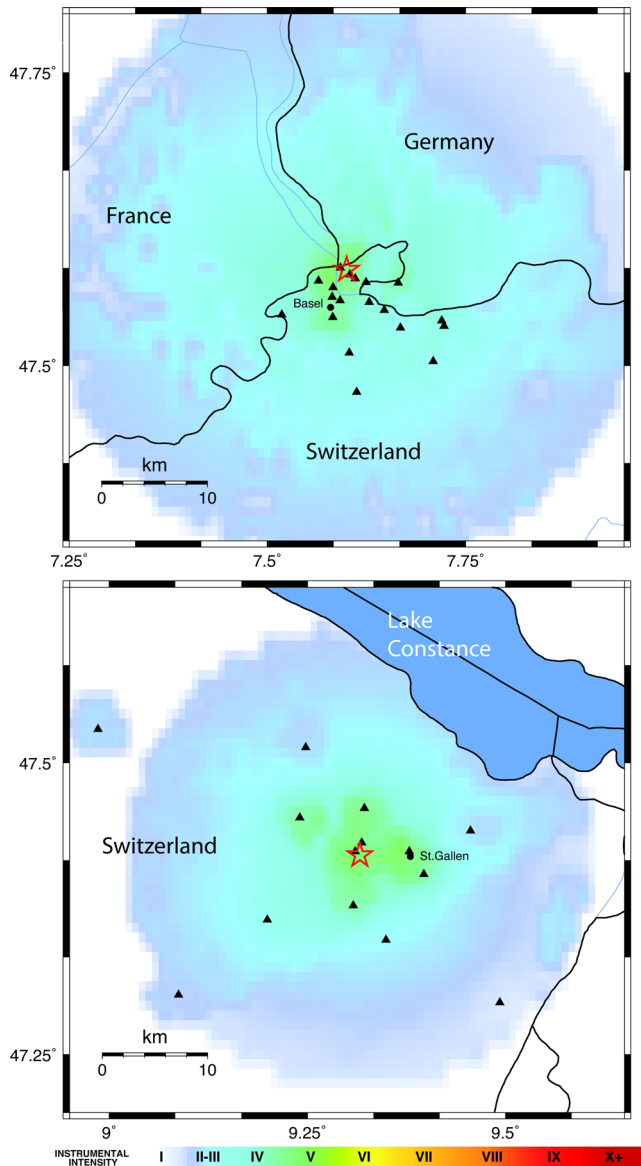


Figure 12. ShakeMaps for the Basel 2006 $M_w = 3.2$ event (top panel) and the St Gallen 2013 $M_w = 3.4$ earthquake bottom panel. In each panel, the red star is the location of the epicentre and the triangles represent the seismic stations recording the event. Administrative boundaries are depicted as black solid curves. Colours are proportional to EMS-98 intensity levels, computed as explained in the text.

questionnaires were available, leading to large uncertainties in the intensity assignments (these are marked as ‘felt’ in Fig. 13). There were no areas with returned questionnaires that could be confidently assigned ‘not-felt’. This is not untypical for small events at night: Intensity III is hardly detectable, as sleeping people do not generally wake up from this level of shaking. However, due to the lack of fully systematic sampling, the proportion of the population is unknown. Intensity 5 was not reached, as the event was not predominantly perceived as frightening; triggering people to leave their buildings, while even minor damage to poorly constructed buildings was not reported to a statistically significant level.

Comparing the macroseismic observations to the 2006 Basel event, the sampling and analysis of macroseismic information was done identically. Comparing the macroseismic fields shows that the Basel event resulted in higher intensities, up to V, in some regions

of the epicentral area. Despite the definition of EMS-Intensity V relating to ‘slight-damage’, the significant number of claims associated to the high population exposure of a shallow seismic event beneath the city led to total damages of \$7.5M. Whilst the recorded ground-motions, discussed previously, showed only small average differences at long-period (e.g. 1 s) motion, an important question is whether the Basel event actually triggered stronger *perceptible* shaking. The Basel event shows, based on 808 questionnaires, of which 769 report the earthquake as being felt, not only higher maximum intensities, but also a larger felt area: In Basel, 7.15 per cent of the felt reports came from areas further than 15 km from the epicentre, and 2.34 per cent from further than 20 km. In St Gallen, these values are 2.65 per cent and 0.79 per cent, respectively. This observation is entirely consistent with the ShakeMap scenarios (Fig. 12). However, macroseismic surveys may be susceptible to external factors. While the population distribution would not explain the different results, comparing a night event to a day event might have significant impact: while at night, the share of the sleeping population waking up from the shaking is an important argument for distinguishing intensities III to V. For a daytime event the distinction is made based on the level of alertness, and the impact of the shaking to objects (beyond the mere human sensation of the tremor). Thus, the same intensities may represent different classes of observations.

As for the events under discussion, observations are described by the same questionnaires. There is therefore an opportunity to go back to the statistical assessment of individual phenomena observed in the same distance of the epicentre in order to limit the effects of night versus day events. To do so, we compared the reports collected from a circle with 8 km radius, comprising 593 (Basel) and 300 (St Gallen) questionnaires. We looked only at those questionnaires which reported the earthquake to have been felt.

In terms of human perception, in Basel, the earthquake was more often reported to be strong or very strong (Fig. 14). At the same time, in St Gallen, people report more often that the shaking was felt by ‘a few’, while in Basel, it was predominantly felt by ‘many’ or ‘almost all’. People in St Gallen were less surprised (56 per cent compared to 71 per cent), less frightened (13 per cent compared to 46 per cent), and less inclined to leave the building to protect from damage (1 per cent compared to 5 per cent). These observations are not biased by the share of reporting people being in buildings rather than outside (this share is >95 per cent in both cases). Neither does it depend on the level on which people live: respondents in St Gallen live significantly less often on the first upper floor, but more often on the second or third floor. In upper floors, higher shaking amplitudes are expected, due to amplification effects within the buildings (Michel *et al.* 2010).

Beside different shaking levels, these differences could depend on the time of the day (lower readiness to become uneasy at night than during daytime) or by the fact that the Basel event caught most people by surprise. For instance, in St Gallen, many people already knew at least theoretically that induced earthquakes were possible due to the previous experience of the Basel event and the extensive media attention. In order to disassociate the analysis from psychological effects, one can look at effects on objects rather than on humans. China and glassware were reported to clink together significantly more often in Basel (35 per cent compared to 17 per cent). Also windows and doors were more frequently reported to rattle in Basel (32 per cent compared to 25 per cent). In contrast, creaking woodwork was more often reported in St Gallen (35 per cent compared to 20 per cent). All these audible effects are probably not significantly affected by the fact that the St Gallen event

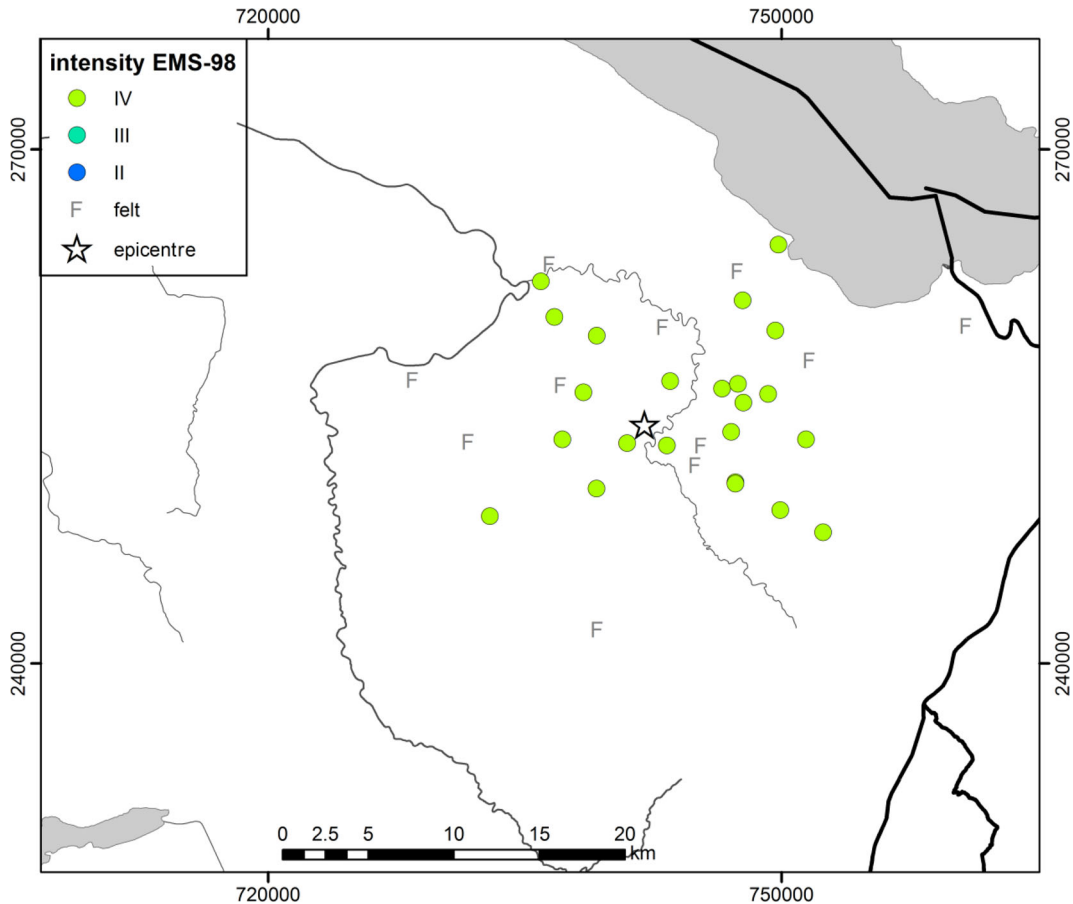


Figure 13. Macroseismic intensity assessment by postal code for the St Gallen $M_L = 3.5$ event. The black lines indicate geographical borders, the grey lines indicate rivers.

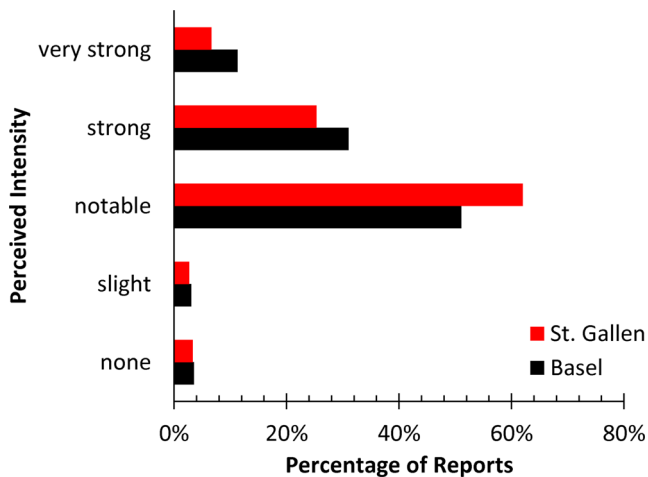


Figure 14. Personal perception of the earthquakes as answered in felt-reports.

happens at night. In contrast, the swinging of suspended objects (lamps, etc.), not perceptible in darkness, is reported more often from Basel (23 per cent) than from St Gallen (12 per cent). However, if looking at the distribution of light versus considerable versus strong swinging, there is no significant difference, indicating that in St Gallen, the effect may have been present, but not often observed due to the darkness.

Earthquake source spectra

In order to improve our understanding of the differences observed between St Gallen and Basel in terms of both instrumental ground-motions and macroseismic intensity we can isolate the contributions of the earthquake sources. The far-field Fourier displacement spectrum for small earthquakes is typically modelled as a convolution of source [$E(f)$], path [anelastic: $B(R, f)$, geometric: $S(R)$] and site effects [$T(f)$], which are multiplied in the frequency domain:

$$\Omega(f) = E(f)B(R, f)S(R)T(f). \tag{8}$$

With the source spectrum modelled as an instantaneous slipping circular fault:

$$E(f) = \frac{\Omega_0}{1 + \left(\frac{f}{f_c}\right)^2}, \tag{9}$$

where Ω_0 is the far-field signal moment and f_c the source corner frequency (Brune 1970). Given two events (labelled 1 and 2) at the same location, recorded at the same site, the ratio of their spectra is given by:

$$\frac{E_1}{E_2}(f) = \frac{\Omega_{0,1} \left[1 + \left(\frac{f}{f_{c,2}}\right)^2\right]}{\Omega_{0,2} \left[1 + \left(\frac{f}{f_{c,1}}\right)^2\right]} \tag{10}$$

with the other terms in eq. (8) cancelling. This approach effectively uses an empirical Green's function (Hartzell 1978) and vastly

simplifies our inversion problem to three terms: $f_{c,1}$, $f_{c,2}$, and the ratio $\frac{\Omega_{0,1}}{\Omega_{0,2}}$. In order to resolve these terms, the corner-frequencies must be sufficiently different. This can be interpreted as requiring two events of sufficiently different magnitude [assuming that $f_c \propto 1/M_0^{1/3}$ (Brune 1970)]. The advantage of using the spectral ratio (empirical Green's function) approach is that any path or site effects are effectively removed so that the typical trade-off problems associated to source retrieval are avoided. This approach could be extended to the smaller shocks, but is beyond the scope of this paper.

To find 'colocated' earthquakes in the relocated Basel event catalogue (Kraft & Deichmann 2014) we searched for locations within $\pm 0.001^\circ$ latitude and longitude (approximately ± 100 m) and ± 100 m in depth. For St Gallen, relocated events were not yet finalized: here we classed events from the routine catalogue within $\pm 0.002^\circ$ latitude and longitude and ± 200 m depth as colocated. In both cases a minimum magnitude difference of 1.5 units was required to ensure a reasonable separation of the corner-frequencies (this corresponds to a factor of approximately 3 in f_c for a constant stress-drop versus magnitude scaling).

For the Basel 'main shock' 14 colocated events (273 record pairs) with magnitudes $M_L = 0.9$ to $M_L = 1.9 \pm 0.15$ were found to match the criteria, while for the St Gallen 'main shock' 11 events (59 record pairs) with magnitudes $M_L = -0.3$ to $M_L = 1.8 \pm 0.15$ were found. The model in eq. (10) was fit between the minimum and maximum frequency limits between which the SNR exceeded 3.

The ratio between the minimum and maximum limits of the frequency bandwidth was required to be at least a factor of 3.2, whilst the maximum and lower limit was 5 Hz and minimum upper limit was 10 Hz. The resulting spectral ratios for Basel are shown in Fig. 15. In Fig. 15(b) all spectral ratios in Fig. 15(a) are normalized to a common reference (arbitrarily $f_{c,2} = 20$ Hz), with $f_{c,1} = 6.7$ Hz corresponding to the best fitting main shock corner frequency.

Fig. 16 shows the spectral ratios between the St Gallen main shock and the colocated events. In Fig. 16(b) the ratios are again normalized to the same reference ($f_{c,2} = 20$ Hz) co-located event with $f_{c,1} = 4.2$ Hz corresponding to the best-fitting main shock corner frequency. Direct comparison between the St Gallen and Basel events is then possible, with the Basel event exhibiting higher-frequency radiated source energy (Fig. 14b: green curve).

Assuming a circular fault the radius of the fault is given by:

$$r_0 = \frac{0.372\beta}{f_c} \quad (11)$$

(Brune 1970, 1971) (with β the shear wave velocity at the source). Stress-drop can then be computed using:

$$\Delta\sigma = \frac{7}{16} \left(\frac{M_0}{r_0^3} \right) \quad (12)$$

(Eshelby 1957). The best-fitting corner frequency (f_c of the Basel event was 6.3 Hz. We define confidence limits using an arbitrary

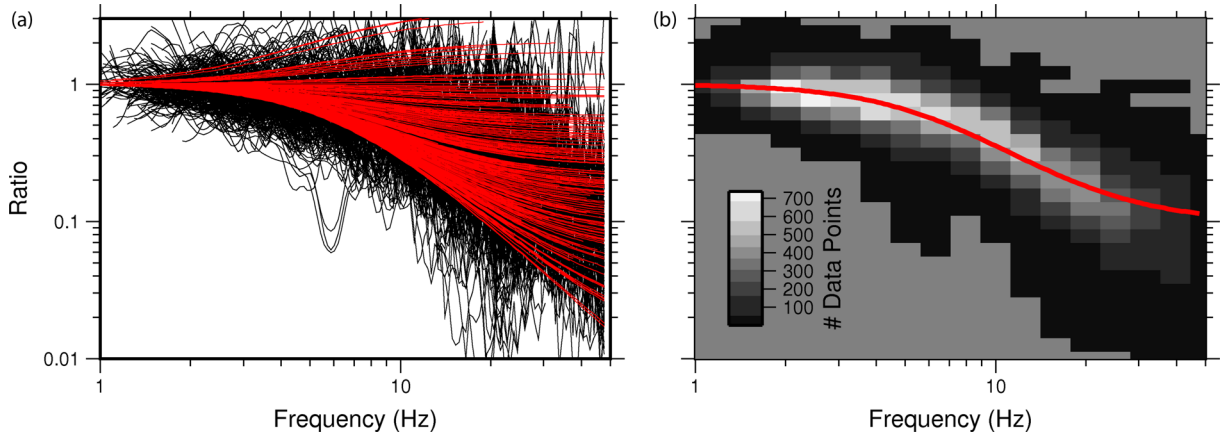


Figure 15. (a) Spectral ratios between the Basel main shock and the small colocated events (black: observed; red: modelled). (b) All spectral ratios normalized to a common colocated event with $f_{c,2} = 20$ Hz (red: normalized model).

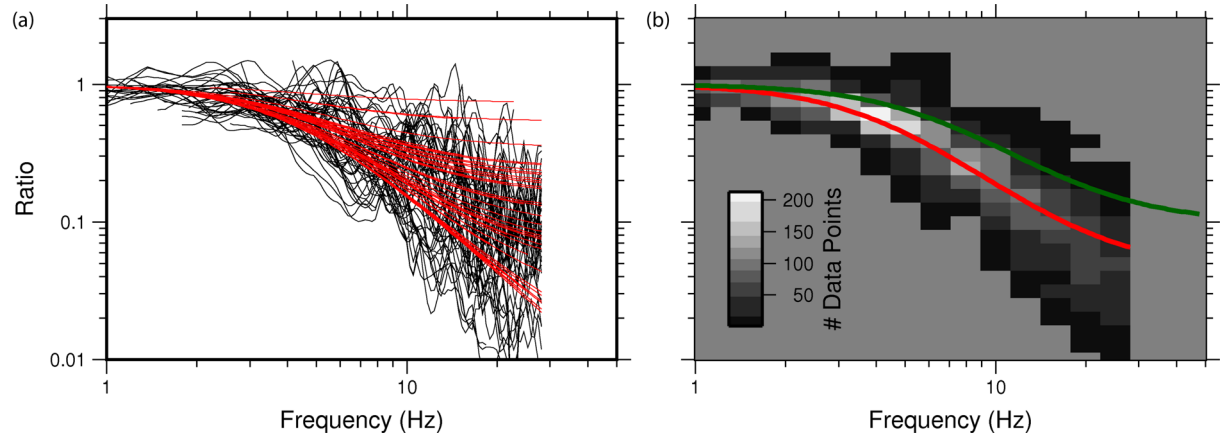


Figure 16. (a) Spectral ratios between the St Gallen main shock and the small colocated events (black: observed; red: modelled). (b) All spectral ratios normalized to a common colocated event with $f_{c,2} = 20$ Hz [red: normalized model; green: normalized Basel model (from Fig. 15)].

tolerance of ± 5 per cent of the minimum least-squares misfit for all corner frequencies (and corresponding fault stress-drops and dimensions) (e.g. Viegas *et al.* 2010). For the Basel event this corresponds to limits of 3.8 and 9.1 Hz. For St Gallen the best-fitting corner-frequency was 4.2 Hz (± 5 per cent f_c misfit limits: 3.4–5.1 Hz). $\beta = 3.5 \text{ km s}^{-1}$ (Dyer *et al.* 2008) in the crystalline basement beneath Basel (Campus & Fah 1997). For a Brune (1970, 1971) source model the resulting circular fault diameter for the Basel event is 410 m (with corresponding ± 5 per cent f_c misfit limits: 290–690 m). Alternatively, using the source model of Haskell (1964) for a square fault with slip velocity of 0.9β (Savage 1972) gives $L = 340 \text{ m}$ (with corresponding ± 5 per cent f_c misfit limits: 240–570 m). In St Gallen the events occur in a medium with $\beta = 3.1 \text{ km s}^{-1}$ (Diehl *et al.* 2014). The diameter using the Brune (1970, 1971) model is larger than for Basel, at 550 m (with corresponding ± 5 per cent f_c misfit limits: 440–680 m). Using the Haskell (1964) model we obtain $L = 450 \text{ m}$ (again larger than the Basel case), with corresponding ± 5 per cent f_c misfit limits: 370–560 m. This is consistent with the fault measurements of approximately $500 \times 400 \text{ m}$ based on illumination by microseismicity (Diehl *et al.* 2014).

Uncertainties in the shear wave velocity in the vicinity of the source propagate into the uncertainty in fault size (e.g. eq. 11), however shear wave velocities at depths of 4–5 km are typically much more certain than source corner-frequencies. For instance, different Swiss bedrock/geology conditions typically show only ± 10 per cent differences in velocity at such depths (Fäh *et al.* 2003; Husen *et al.* 2003; Poggi *et al.* 2011), which translates to approximate additional uncertainty in the fault size of tens of metres. Further uncertainty is introduced if we consider that the fault dimensions depend not only on the source model assumed, but also on the aspect ratio. Such asymmetric faults would also lead to two corner frequencies (Savage 1972), which is beyond the scope of this work to consider. Unfortunately it is not possible to propagate the different sources of uncertainty to provide a total uncertainty in the fault dimensions. It is therefore clear that from this analysis that we cannot conclusively state that one fault is larger than the other. Nevertheless, despite the numerous uncertainties related to defining the fault dimensions, the measurements determined here provide a first order estimate of the expected fault sizes and related uncertainties.

Based on the Brune source model, the resulting stress drops were 3.5 MPa (± 5 per cent f_c misfit limits: 0.76–10.4 MPa) for Basel and 3.0 MPa (± 5 per cent f_c misfit limits: 1.6–5.6 MPa) for St Gallen. While the solutions including uncertainty for the f_c of the two events overlap, the median estimates are clearly different (Fig. 16b). However, translating the f_c into stress drops, the values are very similar (owing to the different velocities at the source region ($\beta = 3.5 \text{ km s}^{-1}$ in Basel compared to $\beta = 3.1 \text{ km s}^{-1}$ in St Gallen)).

The source duration ($1/f_c$) for the St Gallen event is was approximately 50 per cent longer than the Basel event (1/4.2 s compared to 1/6.3 s, respectively). Considering in addition the 11 per cent slower rupture speed in St Gallen this ends in a rupture patch that is 25 per cent larger. Since the magnitude (and therefore seismic moment) of the Basel event was smaller than the St Gallen event the stress drops are similar, and cannot be distinguished considering their uncertainty.

This analysis suggests why the peak motions at high frequency are similar (Fig. 10), despite the different magnitude ($M_w = 3.2$ for Basel and $M_w = 3.4$ for St Gallen). At low frequency (e.g. 1 Hz: Fig. 10d) the dominant effect on ground-motion is driven by magnitude. The St Gallen event therefore exhibits higher long-period ground-motion. However, for higher frequency motions (e.g. PGV, PGA: Figs 10a–b) ground-motion is driven not only by earthquake

magnitude, but also the proportion of high-frequency radiated energy, which is defined by the source corner frequency. The source corner frequency is itself related to stress-drop and rupture velocity (Brune 1970). In this case the stress drop for the Basel and St Gallen events are similar (around 3 MPa), but the higher shear-wave velocity in the Basel source region leads to a higher corner-frequency (or equivalently a shorter source pulse-width). Despite its lower magnitude, the higher corner-frequency of the Basel event increases the ground motion (with respect to the long-period motions), leading to similar levels of shaking to the larger magnitude St Gallen event.

DISCUSSION

The St Gallen geothermal project, and associated seismic monitoring, provided the opportunity to test the seismic monitoring on a small-scale local network. While the routine network of the SED was able to successfully determine the magnitude of the main shock and several of the larger events of the St Gallen sequence, the magnitudes of the smaller events ($M_L < 1.0$) of the sequence were initially significantly overestimated. This was due to the fact that the smaller events were only recorded on the local monitoring network (within a few tens of kilometres). The fact that the existing attenuation correction in the SED local magnitude equation is incorrect for $R < 20 \text{ km}$, and the potential biasing effect of systematic site amplification within such a small region, meant that we had to derive station specific correction factors to obtain robust and accurate magnitudes for the smaller events. Since the larger events (roughly $M_L > 1.3$) were well recorded by the national seismic network and the local network, we could assign average corrections based on the difference between the national and local station specific magnitudes. This led to significant corrections (between -0.2 and -1.3) to the station M_L values determined on the local network.

Using an extended data set of nearly 2700 events, we developed an update for the local magnitude attenuation correction such that it was valid down to 1 km. The updated attenuation correction function can be used for future events, with station corrections only necessary to correct for amplification effects. The updated attenuation correction allowed us to isolate the site amplification contributions to the previously derived station corrections valid for the St Gallen events. The dominant contribution to the station corrections was the bias of the attenuation correction at short distances (with up to 1 unit correction, depending on the distance between the station and the seismic cloud). The correction due to amplification effects was within ± 0.5 units. The station corrections due to amplification effects were found to be consistent with independently derived broad-band amplification functions (Michel *et al.* 2014). This shows that site specific amplification, for example derived from geophysical investigations of the near-surface velocity structure, or based on empirical analysis of seismicity (Edwards *et al.* 2013) can be used in future to estimate the appropriate correction for station specific M_L .

Moment magnitudes were independently determined for the events with M_L down to -1 . The success of the station specific magnitude corrections for the small shocks was obvious when plotting the M_L versus M_w correlation: in the case that no correction (for amplification and the incorrect attenuation correction at the station-seismic cloud distance) was applied, there was limited discernible correlation. However, after station specific M_L corrections were applied, the correlation between M_L and M_w conformed almost exactly to an existing Swiss relation (Goertz-Allmann *et al.* 2011) and indeed many other regions of induced seismicity (Edwards & Douglas 2014). In fact, for the smallest events ($M < 1$), where the

existing M_L : M_w relation was not defined, we saw that the scaling between M_L and M_w was exactly 2/3: a value consistent with other studies of repeating micro-earthquakes and theoretical studies (Hanks & Boore 1984; Edwards *et al.* 2010; Bethmann *et al.* 2011).

TLSs (Bommer *et al.* 2006) or Advanced TLSs (ATLS; Gischig & Wiemer 2013) for induced seismicity rely on seismic monitoring for successful alerting and predictions. Typically, threshold magnitudes are defined consistent with existing codes (e.g. maximum permissible PGV) which can be used alongside ground-motion prediction equations suitable for induced seismicity (Douglas *et al.* 2013). The example presented here shows the importance of considering magnitude determination in addition to location when designing the local monitoring network and preparing analysis tools. Regional seismic monitoring is focussed on larger events, recorded over a wide range of distances. Empirical relations (such as M_L equations) that are calibrated over such distances are not guaranteed to work at the very short distance scales typical when monitoring induced seismicity, as found in this case. Furthermore, the limitation of network size (in order to record the smallest events) means that hard-rock reference stations may not be available: in this case amplification due to local soil or weathered rock may be expected. Clearly such problems can be avoided to a certain extent through the installation of permanent high quality broad-band seismometers in very low noise environments. Such stations are typically located on very hard rock (with limited or no amplification) and can still record small earthquakes at relatively large distances. Practical limitations will of course prevent such stations being used exclusively for microseismicity monitoring. However, seismic observatories should consider the significant advantage of such stations when planning network expansion or renewal in the case that microseismicity monitoring is considered.

In the case of the St Gallen monitoring network, a correction of the empirical magnitude equation was carried out retrospectively using the larger events to determine the local station corrections. This is clearly not ideal in the case where risk analyses are to be carried out prior to production phases. Small events are generated during test phases of geothermal wells; however they cannot be used since reference recordings (e.g. recordings at distance on the wider network) are required. An initial step for future projects, as shown in this work, would be to ensure regional network magnitude equations are correctly calibrated for very short recording distances (using available data from the whole network) before using them during microseismic monitoring. Furthermore, site amplification can be estimated using non-invasive geophysical approaches (Michel *et al.* 2014) as undertaken for all new stations of the permanent seismic networks in Switzerland. Such approaches have been shown to successfully account for the 1-D amplification behaviour of the local subsurface (Edwards *et al.* 2013) and can be undertaken for relatively little cost. Direct estimation of amplification effects is also possible directly from seismic monitoring (Edwards *et al.* 2013) or using site to reference spectral ratios (Borcherdt 1970) in the case of a nearby hard-rock reference such as a deep borehole. Such approaches rely on interfacing the temporary monitoring network with the wider regional seismic networks and analysing the site's response to local and regional small earthquakes (e.g. $M_L > 2.5$) with reference to the wider network or the reference site. This can be achieved for even lower costs, but requires co-ordination with regional seismic observatories and the installation of the monitoring network for a sufficient time (to record background seismicity) prior to any analysis. Nevertheless, Edwards & Douglas (2013) showed that in the case of a geothermal project in Cooper Basin, Australia, the estimation of source, attenuation and site amplification

terms was stable after a relatively small number of events had been recorded (e.g. of the order tens of events), but clearly this depends on the variability of level of seismicity and ground motion in the study area.

The comparison of ground motion produced during the Basel and St Gallen geothermal projects gives an interesting insight into the dependence of ground-motion not only on fault area and slip (i.e. seismic moment), but also radiated energy. In principal, one would expect larger magnitude events to produce higher ground-motions (e.g. Akkar & Bommer 2010). This is indeed the case for relatively long period motions (e.g. $T \geq 1$ s). However, for increasingly shorter period ground motion, up to PGA, the role of fault kinematics (slip velocity or stress-drop) increasingly matters. This was observed when comparing the $M_w = 3.2$ Basel main shock with the $M_w = 3.4$ St Gallen main shock. For the short periods, the ground motion was similar, whilst for long periods the St Gallen event produced, on average, stronger shaking. This can be explained by the fact that the source corner frequency (defining the relative proportion of high-frequency radiated energy) for the Basel event was higher, as shown though an empirical Green's function based deconvolution of the source spectra. Interestingly, this is also reflected in the different magnitude scales (for Basel $M_L = 3.4 \pm 0.1$ and $M_w = 3.2 \pm 0.1$ and St Gallen $M_L = 3.5 \pm 0.1$ and $M_w = 3.4 \pm 0.1$). For M_L , which is more sensitive to higher-frequency ground-motion, the difference between the events reduced to 0.1, reflecting the limited difference in ground-motion at higher frequencies (e.g. PGV, PGA).

An important question related to shallow induced seismicity is whether *perceived* shaking for the two similarly sized events was stronger in Basel than in St Gallen? Whilst the instrumental data does not show a clear systematic distinction, from the macroseismic survey it can be concluded that the Basel event was at least more strongly felt. The difference may be related to be in the relative frequency content of the signals: effects requiring high-frequency excitation, such as rattling of china, windows and doors, are clearly predominant in Basel, while effects which may also be triggered from lower frequency excitation ($f < 10$ Hz), such as creaking woodwork and swinging objects, show a more balanced image. This is consistent with two aspects of human perception: (i) eyewitnesses of the Basel event describe the motion as shaking (88 per cent) rather than swinging (7 per cent), while in St Gallen, the difference was somewhat less distinct (81 per cent versus 15 per cent); (ii) in their free text comments, many (>10 per cent) people from Basel reported their quake to be accompanied by an audible bang, whilst hardly anybody in St Gallen report similar observations. What is interesting, and relevant for future macroseismic research, is the fact that these relatively small differences of otherwise similar earthquakes are clearly observable from macroseismic observations, if the analyst goes from looking at intensities to looking at the perception of individual phenomena.

The overall similarity in absolute amplitudes of ground-motion does not help to easily explain why the Basel event caused widespread minor damage. However, both the ShakeMaps and observed macroseismic reports for the two events do indicate that the felt intensity field for the Basel event extended far wider than the St Gallen event. Additionally, in Basel at one station (SBEG) significant peaks in the response spectral amplitudes within the range of the typical response of low-rise buildings were observed, leading to exceptional levels of ground-motion (well above other stations at similar distances). These effects could not be entirely explained by average local amplification, and may indicate source directivity, or atypical local site effects. It is known that the ability of a local monitoring network to capture the full range of variability of a

ground-motion field is difficult. In fact, Douglas (2013) showed that very high network densities of up to 50–100 stations km^{-2} would be needed to ‘fully’ record a spatially correlated ground-motion field. Therefore, one might expect other isolated regions of very high ground-motion (unobserved by the local monitoring network) to exist. However, this could equally be said of the St Gallen event. In terms of vulnerability some of the building stock in Basel is known to have problems: results presented by Lang (2002) revealed that ‘due to unsuitable building layout (soft storeys, no lateral force resisting elements in one direction) buildings dating from the 1960s with a mixed system of vertical reinforced concrete elements combined with un-reinforced masonry elements having reinforced concrete floors are extremely vulnerable to seismic lateral forces, even more than pure unreinforced masonry buildings’. However, whether such assessments extend to relatively weak ground-motions and minor structural damage is questionable. Nevertheless, if we consider the combined factors in Basel of a more energetic event, the increased extent and characteristics of the reported macroseismic field and ShakeMap intensities, in addition to the influence of wider exposure, it may help to explain the higher damage level.

ACKNOWLEDGEMENTS

This work was partially funded by St Gallen Stadtwerk within the context of the GEOSIM project, the GEOBEST project and the Swiss Federal Nuclear Safety Inspectorate (ENSI). We would like to thank the two reviewers, Gail Atkinson and Joachim Ritter, for their thorough reviews of this manuscript which have helped to improve the paper.

REFERENCES

- Akkar, S. & Bommer, J.J., 2010. Empirical equations for the prediction of PGA, PGV, and spectral accelerations in Europe, the Mediterranean region, and the Middle East, *Seismol. Res. Lett.*, **81**, 195–206.
- Atkinson, G., 2015. Ground-motion prediction equation for small-to-moderate events at short hypocentral distances, with application to induced-seismicity hazards, *Bull. seism. Soc. Am.*, doi:10.1785/0120140142.
- Bachmann, C.E., Wiemer, S., Woessner, J. & Hainzl, S., 2011. Statistical analysis of the induced Basel 2006 earthquake sequence: Introducing a probability-based monitoring approach for enhanced geothermal systems, *Geophys. J. Int.*, **186**, 793–807.
- Baer, M. *et al.*, 2007. Earthquakes in Switzerland and surrounding regions during 2006, *Swiss J. Geosci.*, **100**, 517–528.
- Bay, F., Wiemer, S., Fäh, D. & Giardini, D., 2005. Predictive ground motion scaling in Switzerland: best estimates and uncertainties, *J. Seismol.*, **9**, 223–240.
- Bethmann, F., Deichmann, N. & Mai, P.M., 2011. Scaling relations of local magnitude versus moment magnitude for sequences of similar earthquakes in Switzerland, *Bull. seism. Soc. Am.*, **101**, 515–534.
- Blanpied, M.L., Lockner, D.A. & Byerlee, J.D., 1992. An earthquake mechanism based on rapid sealing of faults, *Nature*, **358**, 574–576.
- Bommer, J.J., Oates, S., Cepeda, J.M., Lindholm, C., Bird, J., Torres, R., Marroquin, G. & Rivas, J., 2006. Control of hazard due to seismicity induced by a hot fractured rock geothermal project, *Eng. Geol.*, **83**, 287–306.
- Borcherdt, R.D., 1970. Effects of local geology on ground motion near San Francisco Bay, *Bull. seism. Soc. Am.*, **60**, 29–61.
- Brune, J.N., 1970. Tectonic stress and spectra of seismic shear waves from earthquakes, *J. geophys. Res.*, **75**, 4997–5009.
- Brune, J.N., 1971. Correction to “Tectonic stress and the spectra, of seismic shear waves from earthquakes”, *J. geophys. Res.*, **76**, 5002, doi:10.1029/JB076i020p05002.
- Campus, P. & Fah, D., 1997. Seismic monitoring of explosions: a method to extract information on the isotropic component of the seismic source, *J. Seismol.*, **1**, 205–218.
- Cauzzi, C. & Clinton, J., 2013. A high- and low-noise model for high-quality strong-motion accelerometer stations, *Earthq. Spectra*, **29**, 85–102.
- Cauzzi, C., Clinton, J., Becker, J. & Kaestli, P., 2013. Scwffparam: a tool for rapid parameterisation of ground motions and input to ShakeMap in SeisComp3, in *Proceedings of the Seismological Society of America Annual Meeting*, Salt Lake City, UT, USA.
- Cauzzi, C., Edwards, B., Fäh, D., Clinton, J., Wiemer, S., Kästli, P., Cua, G. & Giardini, D., 2015. New predictive equations and site amplification estimates for the next-generation Swiss ShakeMaps, *Geophys. J. Int.*, **200**, 421–438.
- CEN, 2004. Eurocode 8: design of structures for earthquake resistance – Part 1: general rules, seismic actions and rules for buildings, in *Proceedings of the Eurocode 8*, European Committee for Standardization, Brussels.
- Clinton, J. *et al.*, 2011. The current state of strong motion monitoring in Switzerland, in *Earthquake Data in engineering Seismology: Predictive Models, Data Management and Networks*, pp. 219–233, eds Akkar, S., Gülkan, P. & Eck, T.V., Springer.
- Cloetingh, S. *et al.*, 2010. Lithosphere tectonics and thermo-mechanical properties: an integrated modelling approach for enhanced geothermal systems exploration in Europe, *Earth-Sci. Rev.*, **102**, 159–206.
- Deichmann, N., 2006. Local magnitude, a moment revisited, *Bull. seism. Soc. Am.*, **96**, 1267–1277.
- Diehl, T. *et al.*, 2013. Earthquakes in Switzerland and surrounding regions during 2012, *Swiss J. Geosci.*, **106**, 543–558.
- Diehl, T., Kraft, T., Eduard, K., Nicholas, D., Clinton, J. & Wiemer, S., 2014. High-precision relocation of induced seismicity in the geothermal system below St. Gallen (Switzerland), in EGU General Assembly Conference Abstracts, 12541.
- Dost, B., Van Eck, T. & Haak, H., 2004. Scaling of peak ground acceleration and peak ground velocity recorded in the Netherlands, *Bollettino Di Geofisica Teorica Ed Applicata*, **45**, 153–168.
- Douglas, J., 2013. Seismic network design to detect felt ground motions from induced seismicity, *Soil Dyn. Earthq. Eng.*, **48**, 193–197.
- Douglas, J. *et al.*, 2013. Predicting ground motion from induced earthquakes in geothermal areas, *Bull. seism. Soc. Am.*, **103**, 1875–1897.
- Dyer, B., Schanz, U., Ladner, F., Häring, M. & Spillman, T., 2008. Micro-seismic imaging of a geothermal reservoir stimulation, *Leading Edge*, **27**, 856–869.
- Edwards, B. & Douglas, J., 2013. Selecting ground-motion models developed for induced seismicity in geothermal areas, *Geophys. J. Int.*, **195**, 1314–1322.
- Edwards, B. & Douglas, J., 2014. Magnitude scaling of induced earthquakes, *Geothermics*, **52**, 132–139.
- Edwards, B. & Fäh, D., 2013. A stochastic ground-motion model for Switzerland, *Bull. seism. Soc. Am.*, **103**, 78–98.
- Edwards, B., Allmann, B., Fäh, D. & Clinton, J., 2010. Automatic computation of moment magnitudes for small earthquakes and the scaling of local to moment magnitude, *Geophys. J. Int.*, **183**, 407–420.
- Edwards, B., Fäh, D. & Giardini, D., 2011. Attenuation of seismic shear wave energy in Switzerland, *Geophys. J. Int.*, **185**, 967–984.
- Edwards, B., Michel, C., Poggi, V. & Fäh, D., 2013. Determination of site amplification from regional seismicity: application to the Swiss National Seismic Networks, *Seismol. Res. Lett.*, **84**, 611–621.
- Ellsworth, W.L., 2013. Injection-induced earthquakes, *Science*, **341**, 142, doi:10.1126/Science.1225942.
- Eshelby, J.D., 1957. The determination of the elastic field of an ellipsoidal inclusion, and related problems, *Proc. R. Soc. Lond., A: Math. Phys. Sci.*, **241**, 376–396.
- Faenza, L. & Michelini, A., 2010. Regression analysis of MCS intensity and ground motion parameters in Italy and its application in ShakeMap, *Geophys. J. Int.*, **180**, 1138–1152.
- Fäh, D., Kind, F. & Giardini, D., 2003. Inversion of local S-wave velocity structures from average H/V ratios, and their use for the estimation of site-effects, *J. Seismol.*, **7**, 449–467.

- Fäh, D. *et al.*, 2011. Ecos-09 earthquake catalogue of Switzerland release 2011 report and database. Public catalogue, 17.4.2011. Swiss Seismological Service, Eth, Zurich, pp. 42.
- Faulkner, D.R., Jackson, C.A.L., Lunn, R.J., Schlische, R.W., Shipton, Z.K., Wibberley, C.A.J. & Withjack, M.O., 2010. A review of recent developments concerning the structure, mechanics and fluid flow properties of fault zones, *J. Struct. Geol.*, **32**, 1557–1575.
- Fridleifsson, I.B., 2001. Geothermal energy for the benefit of the people, *Renew. Sustain. Ener. Rev.*, **5**, 299–312.
- Giardini, D., 2009. Geothermal quake risks must be faced, *Nature*, **462**, 848–849.
- Gischig, V.S. & Wiemer, S., 2013. A stochastic model for induced seismicity based on non-linear pressure diffusion and irreversible permeability enhancement, *Geophys. J. Int.*, **194**, 1229–1249.
- Goertz-Allmann, B.P. & Wiemer, S., 2012. Geomechanical modeling of induced seismicity source parameters and implications for seismic hazard assessment, *Geophysics*, **78**, KS25–KS39.
- Goertz-Allmann, B.P., Edwards, B., Bethmann, F., Deichmann, N., Clinton, J., Fäh, D. & Giardini, D., 2011. A new empirical magnitude scaling relation for Switzerland, *Bull. seism. Soc. Am.*, **101**, 3088–3095.
- Grunthal, G., 1998. *European Macroseismic Scale EMS-98*, Vol. 15, Cahier du Centre Européen de Géodynamique et de Séismologie.
- Grünthal, G., Levret, A., Musson, R. & Schwarz, J., 2001. *L'échelle Macrossismique Européenne (EMS-98)*, Cahiers du Centre européen de géodynamique et de séismologie.
- Grünthal, G., Wahlstrom, R. & Stromeyer, D., 2009. The unified catalogue of earthquakes in central, northern, and northwestern Europe (CENEC)-updated and expanded to the last millennium, *J. Seismol.*, **13**, 517–541.
- Gutenberg, B. & Richter, C.F., 1944. Frequency of earthquakes in California, *Bull. seism. Soc. Am.*, **34**, 185–188.
- Hanka, W., Saul, J., Weber, B., Becker, J., Harjadi, P., & Fauzi GITEWS Seismology Group, 2010. Real-time earthquake monitoring for tsunami warning in the Indian Ocean and beyond, *Nat. Hazards Earth Syst. Sci.*, **10**, 2611–2622.
- Hanks, T.C. & Boore, D.M., 1984. Moment-magnitude relations in theory and practice, *J. geophys. Res.*, **89**, 6229–6235.
- Hanks, T.C. & Kanamori, H., 1979. Moment magnitude scale, *J. geophys. Res.*, **84**, 2348–2350.
- Häring, M.O., Schanz, U., Ladner, F. & Dyer, B.C., 2008. Characterisation of the Basel 1 enhanced geothermal system, *Geothermics*, **37**, 469–495.
- Hartzell, S.H., 1978. Earthquake aftershocks as greens functions, *Geophys. Res. Lett.*, **5**, 1–4.
- Haskell, N.A., 1964. Total energy and energy spectral density of elastic wave radiation from propagating faults, *Bull. seism. Soc. Am.*, **54**, 1811–1841.
- Henderson, J., Barton, D. & Foulger, G., 1999. Fractal clustering of induced seismicity in the Geysers geothermal area, California, *Geophys. J. Int.*, **139**, 317–324.
- Husen, S., Kissling, E., Deichmann, N., Wiemer, S., Giardini, D. & Baer, M., 2003. Probabilistic earthquake location in complex three-dimensional velocity models: application to Switzerland, *J. geophys. Res.: Solid Earth*, **108**, doi:10.1029/2002jb001778.
- Kästli, P. & Fäh, D., 2006. Rapid estimation of macroseismic effects and shake maps combining macroseismic and instrumental data, in *Proceedings of the First European Conference on Earthquake Engineering and Seismology (ECEES)*, Geneva, Switzerland.
- Kisslinger, C., 1976. Theories of mechanisms of induced seismicity, *Eng. Geol.*, **10**, 85–98.
- Kradolfer, U., 1984. *Magnitudenkalibrierung von erdbebenstationen in der schweiz*, ETH, Zurich.
- Kraft, T. & Deichmann, N., 2014. High-precision relocation and focal mechanism of the injection-induced seismicity at the Basel EGS, *Geothermics*, **52**, 59–73.
- Kraft, T., Mignan, A. & Giardini, D., 2013. Optimization of a large-scale microseismic monitoring network in northern Switzerland, *Geophys. J. Int.*, **195**, 474–490.
- Lang, A., 2002. Seismic vulnerability of existing buildings, *PhD thesis*, Swiss Federal Institute of Technology, Zürich.
- Lomax, A., Virieux, J., Volant, P. & Berge-Thierry, C., 2000. Probabilistic earthquake location in 3D and layered models, in *Advances in Seismic Event Location*, pp. 101–134, eds Thurber, C. & Rabinowitz, N., Springer.
- Michel, C., Gueguen, P., El Arem, S., Mazars, J. & Kotronis, P., 2010. Full-scale dynamic response of an RC building under weak seismic motions using earthquake recordings, ambient vibrations and modelling, *Earthq. Eng. Struct. Dyn.*, **39**, 419–441.
- Michel, C., Edwards, B., Poggi, V., Burjanek, J., Roten, D., Cauzzi, C. & Fäh, D., 2014. Assessment of site effects in alpine regions through systematic site characterization of seismic stations, *Bull. seism. Soc. Am.*, **104**, doi:10.1785/0120140097.
- Nanjo, K.Z., Schorlemmer, D., Woessner, J., Wiemer, S. & Giardini, D., 2010. Earthquake detection capability of the Swiss Seismic Network, *Geophys. J. Int.*, **181**, 1713–1724.
- Ottmoller, L. & Havskov, J., 2003. Moment magnitude determination for local and regional earthquakes based on source spectra, *Bull. seism. Soc. Am.*, **93**, 203–214.
- Poggi, V., Edwards, B. & Fäh, D., 2011. Derivation of a reference shear-wave velocity model from empirical site amplification, *Bull. seism. Soc. Am.*, **101**, 258–274.
- Richter, C.F., 1935. An instrumental earthquake magnitude scale, *Bull. seism. Soc. Am.*, **25**, 1–32.
- Savage, J.C., 1972. Relation of corner frequency to fault dimensions, *J. geophys. Res.*, **77**, 3788–3795.
- Scherbaum, F., 1990. Combined inversion for the three-dimensional q structure and source parameters using microearthquake spectra, *J. geophys. Res.: Solid Earth (1978–2012)*, **95**, 12 423–12 438.
- Shapiro, S., Dinske, C. & Kummerow, J., 2007. Probability of a given-magnitude earthquake induced by a fluid injection, *Geophys. Res. Lett.*, **34**, doi:10.1029/2007GL031615.
- Steidl, J.H., Tumarkin, A.G. & Archuleta, R.J., 1996. What is a reference site, *Bull. seism. Soc. Am.*, **86**, 1733–1748.
- Taron, J. & Elsworth, D., 2009. Thermal-hydrologic-mechanical-chemical processes in the evolution of engineered geothermal reservoirs, *Int. J. Rock Mech. Mining Sci.*, **46**, 855–864.
- Uhrhammer, R.A. & Collins, E.R., 1990. Synthesis of Wood-Anderson seismograms from broadband digital records, *Bull. seism. Soc. Am.*, **80**, 702–716.
- Viegas, G., Abercrombie, R.E. & Kim, W.Y., 2010. The 2002 m5 Au Sable Forks, NY, earthquake sequence: source scaling relationships and energy budget, *J. geophys. Res.: Solid Earth*, **115**, B07310, doi:10.1029/2009jb006799.
- Wald, D.J., Quitoriano, V., Heaton, T.H., Kanamori, H., Scrivner, C.W. & Worden, C.B., 1999. Trinet “ShakeMaps”: rapid generation of peak ground motion and intensity maps for earthquakes in southern California, *Earthq. Spectra*, **15**, 537–555.
- Wald, D.J., Worden, B.C., Quitoriano, V. & Pankow, K.L., 2005. ShakeMap Manual: Technical Manual, User’s Guide, and Software Guide, US Geological Survey.
- Worden, C., Wald, D., Allen, T., Lin, K., Garcia, D. & Cua, G., 2010. A revised ground-motion and intensity interpolation scheme for ShakeMap, *Bull. seism. Soc. Am.*, **100**, 3083–3096.
- Worden, C.B., Gerstenberger, M.C., Rhoades, D.A. & Wald, D.J., 2012. Probabilistic relationships between ground-motion parameters and modified Mercalli intensity in California, *Bull. seism. Soc. Am.*, **102**, 204–221.